tvst

Article

When Is a Control Not a Control? Reactive Microglia Occur Throughout the Control Contralateral Pathway of Retinal Ganglion Cell Projections in Experimental Glaucoma

James R. Tribble[1,*], Eirini Kokkali[2,*], Amin Otmani[1], Flavia Plastino[1], Emma Lardner[1], Rupali Vohra[3,4], Miriam Kolko[4,5], Helder André[1], James E. Morgan[2,6], and Pete A. Williams[1]

[1] Department of Clinical Neuroscience, Division of Eye and Vision, St. Erik Eye Hospital, Karolinska Institutet, Stockholm, Sweden
[2] School of Optometry and Vision Sciences, Cardiff University, Cardiff, Wales, UK
[3] Department of Veterinary and Animal Sciences, Pathobiological Sciences, University of Copenhagen, Denmark
[4] Department of Drug Design and Pharmacology, University of Copenhagen, Copenhagen, Denmark
[5] Department of Ophthalmology, Rigshospitalet-Glostrup, Copenhagen, Denmark
[6] School of Medicine, Cardiff University, Cardiff, Wales, UK

Correspondence: Pete A. Williams, Department of Clinical Neuroscience, Division of Eye and Vision, St. Erik Eye Hospital, Karolinska Institutet, Stockholm, Sweden. e-mail: pete.williams@ki.se

Received: May 29, 2020
Accepted: December 2, 2020
Published: January 12, 2021

Keywords: microglia; monocyte; neuroinflammation; glaucoma; retina; optic nerve; optic nerve head; lateral geniculate nucleus; superior colliculus

Citation: Tribble JR, Kokkali E, Otmani A, Plastino F, Lardner E, Vohra R, Kolko M, André H, Morgan JE, Williams PA. When is a control not a control? reactive microglia occur throughout the control contralateral pathway of retinal ganglion cell projections in experimental glaucoma. Trans Vis Sci Tech. 2021;10(1):22, https://doi.org/10.1167/tvst.10.1.22

Purpose: Animal models show retinal ganglion cell (RGC) injuries that replicate features of glaucoma and the contralateral eye is commonly used as an internal control. There is significant crossover of RGC axons from the ipsilateral to the contralateral side at the level of the optic chiasm, which may confound findings when damage is restricted to one eye. The effect of unilateral glaucoma on neuroinflammatory damage to the contralateral pathway of RGC projections has largely been unexplored.

Methods: Ocular hypertensive glaucoma was induced unilaterally or bilaterally in the rat and RGC neurodegenerative events were assessed. Neuroinflammation was quantified in the retina, optic nerve head, optic nerve, lateral geniculate nucleus, and superior colliculus by high-resolution imaging, and in the retina by flow cytometry and protein arrays.

Results: After ocular hypertensive stress, peripheral monocytes enter the retina and microglia become reactive. This effect is more marked in animals with bilateral ocular hypertensive glaucoma. In rats where glaucoma was induced unilaterally, there was significant microglia activation in the contralateral (control) eye. Microglial activation extended into the optic nerve and terminal visual thalami, where it was similar across hemispheres in unilateral ocular hypertension.

Conclusions: These data suggest that caution is warranted when using the contralateral eye as a control and in comparing visual thalami in unilateral models of glaucoma.

Translational Relevance: The use of a contralateral eye as a control may confound the discovery of human-relevant mechanism and treatments in animal models. We also identify neuroinflammatory protein responses that warrant further investigation as potential disease-modifiable targets.

Introduction

Glaucoma is the leading cause of irreversible blindness, affecting approximately 80 million people worldwide.[1] Glaucoma is characterized by the progressive dysfunction and loss of retinal ganglion cells (RGC) and their axons. Neuroinflammation is a shared feature of glaucoma pathogenesis in human glaucoma patients[2] and animal models of glaucoma (genetic and inducible).[3] In times of stress, RGCs are reliant on a supportive network of glial cells to provide

neurotrophic and metabolic support, especially to their long, unmyelinated axons in the retina and optic nerve head. Emerging evidence supports a paradigm in which RGC axons are insulted throughout their trajectory to retinorecipient areas; the dorsal lateral geniculate nucleus (dLGN) and the superior colliculus (SC). Microglia and/or other immune-derived cells are likely to be key players in these pathogenic events.

The eye is commonly used as a tool to explore neurodegenerative events. However, a common feature of these experiments is the use of the contralateral eye as an internal control (which is often used to normalize data to the experimental eye). These data should be qualified because (i) RGC numbers differ between eyes even within individual animals,[4] (ii) significant numbers of RGC axons do not cross at the optic chiasm and terminate in ipsilateral thalami (ranging from approximately 3% in mouse and approximately 3%–10% in rat to approximately 45% in primates and approximately 50% in human),[5–7] (iii) albino rodents are commonly used (e.g., Wistar and Sprague-Dawley rats), which have decreased ipsilateral projections,[8–11] (iv) most human primary open-angle glaucoma is bilateral, and (v) there is evidence of immune activation in the normotensive (NT) contralateral eye.

Microglial activation is an early and persistent feature across glaucoma models and species with evidence of immune cell activation in human tissue from advanced glaucoma.[12–16] Gallego et al.[12] were the first to report observations of immune activation in a unilateral glaucoma model. They demonstrated upregulated major histocompatibility complex class II and a qualitative increase in microglial density in naïve eyes contralateral to the eye induced with ocular hypertension (OHT). These changes in the contralateral eye are likely the result of the OHT, not the induction procedure, as reported by Kezic et al.,[13] who observed no detectable immune effect in eyes contralateral to cannulated control eyes (i.e., anterior chamber injection without pressure modulation). Rojas et al.[14] further explored the contralateral effect on microglia by quantifying increased microglial density, retinal tiling, and reduced arbor size. Ebneter et al.[15] demonstrated that immune activation was not restricted to the contralateral eye, but continued in the optic nerve and optic tract, with Sapienza et al.[16] showing further activation in the SC, thus demonstrating that the phenomenon existed across the RGC trajectory. These studies have focused on RGC–specific tissues (eye, optic nerve, and SC) as a whole, without detailed microglial morphologic analysis. Microglia exhibit broad morphologic diversity under normal physiologic conditions,[17,18] actively remodeling their dendritic processes in response to a number of local stimuli.[19–22] A detailed morphologic analysis of individual microglia is required to better represent their morphologic heterogeneity (in normal and disease conditions) and to more fully appreciate their morphologic responses to OHT across the whole RGC trajectory.

To address these issues and explore neuroinflammation throughout the pathway of RGC projections in glaucoma, we characterize inflammatory changes in an inducible rat model of ocular hypertensive glaucoma in which intraocular pressure (IOP) is increased by intracameral (anterior chamber) injection of paramagnetic beads to occlude the drainage structures of the eye.[23–25] This process results in sustained OHT driving a reproducible and significant loss of RGC numbers as well as neuroinflammation (with no observed uveitis). Using this model, we assessed the effects of unilateral or bilateral induced OHT on glaucoma pathology throughout the RGC projections. These experiments were performed in the Brown Norway rat because it is the genetic standard for rats, inbred, and pigmented, and it avoids the retinothalamic pathway issues present in albino animals. We demonstrate that neuroinflammation persists throughout RGC pathways with monocyte infiltration and proinflammatory cytokine release in the retina. Critically, these changes are consistent with those in the contralateral pathway of RGC projections warranting caution when using the contralateral eye as a control in ophthalmic research. Microglial morphology remains varied, but with a clear shift in population favoring more retracted, voluminous processes consistent with activation, along a gradient of increased neurodegenerative and neuroinflammatory insult.

Methods

Rat Strain and Husbandry

Adult male Brown Norway rats (aged 12–16 weeks, weighing 300–375 g, SCANBUR) were housed and fed in a 12-hour light/12-hour dark cycle with food and water available ad libitum. All experimental procedures were undertaken in accordance with the ARVO Statement for the Use of Animals in Ophthalmic and Research. Individual study protocols were approved by Stockholm's Committee for Ethical Animal Research (10389-2018).

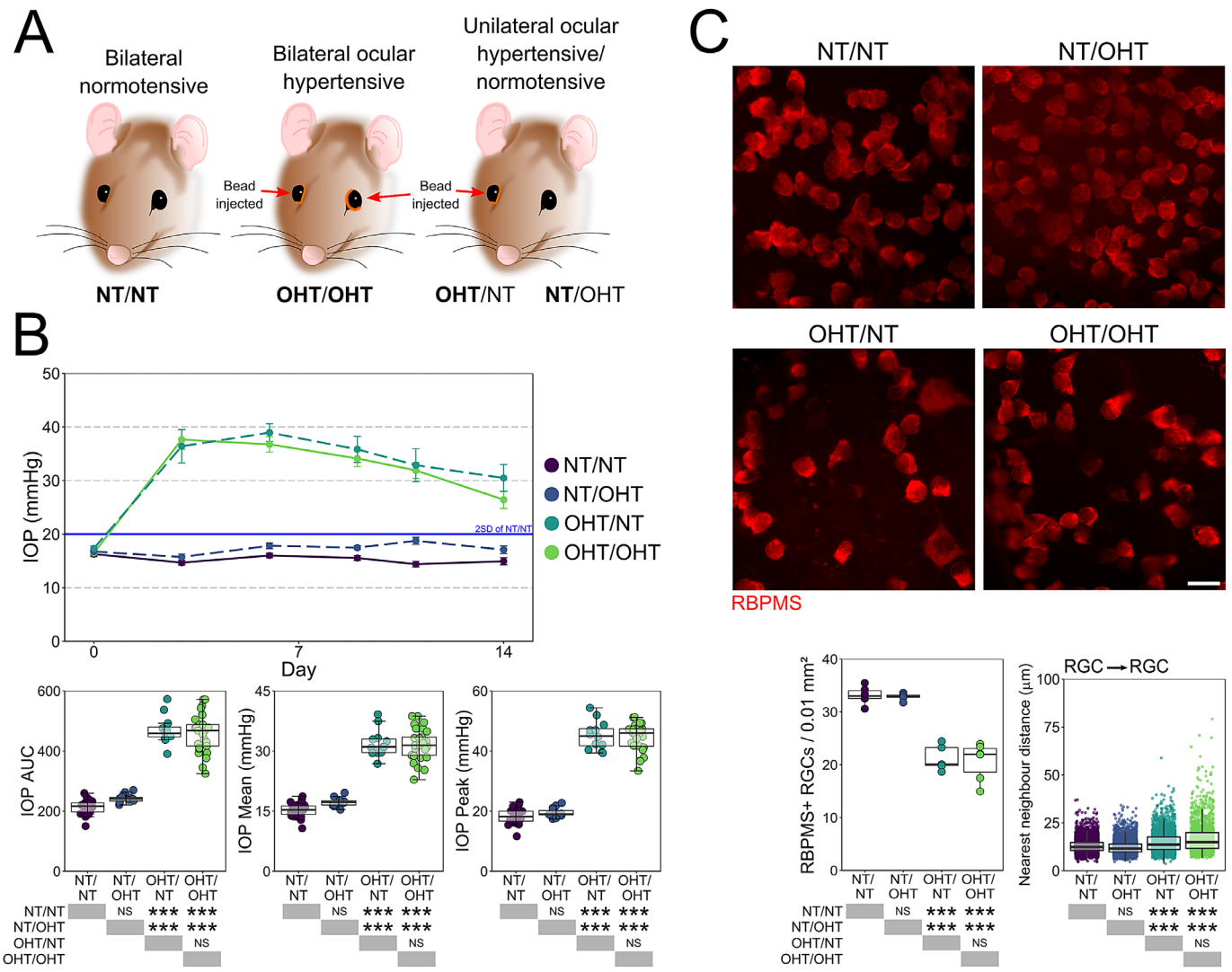

Figure 1. Induction of OHT via paramagnetic bead induction. (**A**) Brown Norway rats underwent intracameral injections of paramagnetic beads either bilaterally or unilaterally. The contralateral eye remained unoperated in unilaterally injected rats. (**B**) Beads were pulled into the drainage structures of the eye via a rare earth magnet resulting in a significant and robust IOP increase that was sustained until euthanasia (**B**). Fourteen days of OHT results in significant RGC atrophy demonstrated in flat-mount retinas, confirming a significant loss of RGCs and increased NND of RGCs after 14 days of OHT. For complete *n* please see Methods. Scale bars = 20 µm in C. $^{*}P < 0.05$, $^{**}P < 0.01$, $^{***}P < 0.001$. NS, not significant ($P > 0.05$).

Induction of OHT

OHT was induced bilaterally (OHT/OHT; n = 9 rats, 18 eyes) or unilaterally (OHT/NT; n = 9 rats, 9 eyes). For unilateral OHT rats, the contralateral eye was an unoperated, NT eye (NT/OHT; n = 9 rats, 9 eyes). Bilateral NT rats served as controls (NT/NT; n = 9 rats, 18 eyes; Fig. 1A). All unilateral eyes were maintained as pairs (i.e., not split for different experiments). OHT was induced using a magnetic microbead injection model as described elsewhere.[25] Microbeads (Dynabead Epoxy M-450, Thermo Fisher, Waltham, MA) were prepared in Hank's Balanced Salt Solution (HBSS) and 6 to 8 µL injected into the anterior chamber. Beads were distributed with a magnet to block the iridocorneal angle. The IOP was measured using a Tonolab rebound tonometer (Icare, Vantaa, Finland) in awake, unrestrained rats, habituated to the tonometry procedure. The baseline IOP was recorded on the day of surgery (day 0) and recorded every 2 to 4 days afterward until the end point (postoperative day 14), with IOP recordings always taken between 9 and 10 AM to avoid the effects of the circadian rhythm on IOP (2–3 hours from lights on). IOP was

Table. Antibody Details

Antibody	Target	Host	Dilution	Details	Use
PE CD11b/c	CD11b (clone OX-42)	Mouse	1:400	Nordic BioSite cat # 201807	FC*
AF 647 CD45	CD45 (clone OX-1)	Mouse	1:2000	Nordic BioSite cat # 202211	FC*
BV 421 CD90.1	Thy1.1 (clone OX-7)	Mouse	1:200	Nordic BioSite cat # 202529	FC*
GS	Glutamine synthethase	Rabbit	1:5000	Sigma-Aldrich cat # G2781	IF†
Isolectin GS-IB_4 (IsoB4)	Poly-N-acetyllactosamine, found on microglia, endothelial cells, monocytes/macrophages	Lectin from Griffonia simplicifolia conjugated to biotin	0.1 mg/mL	Invitrogen cat # I21414	IF†
RBPMS	RNA-binding protein, RGC specific in the retina	Rabbit	1:500	Novusbio cat # NBP2-20112	IF†
Goat-anti Rabbit AF 488	Rabbit primary antibody	Goat	1:500	Abcam cat # A11008	IF†
Goat-anti Rabbit AF 568	Rabbit primary antibody	Goat	1:500	Abcam cat # A11011	IF†
Streptavidin AF 488 conjugate	Biotin	NA	4 µg/mL	Invitrogen cat # S11223	IF†

*FC (flow cytometry).
†IF (immunofluorescence).

taken as the average of five tonometer readings. NT/NT rats followed the same 14-day time course (without surgery). IOP profiles were compared using Kruskal-Wallis test followed by Dunn's tests with Benjamini and Hochberg correction.

General Histopathology

Rats were heavily anaesthetized at day 14 by intraperitoneal injection of pentobarbital (75 mg/kg), and euthanized by cervical dislocation. Eyes were immediately enucleated (with 1 mm of optic nerve post-globe preserved) and immersed in 3.7% PFA in 1× phosphate-buffered saline (PBS). Brains (with attached optic nerves) were removed and immersed in 3.7% PFA in 1× PBS. Eyes, optic nerves, and brains for cryosectioning were maintained in fixative for 24 hours before cryoprotecting in 30% sucrose in 1× PBS for 24 hours, freezing in optimal cutting temperature medium (Sakura) on dry ice, and stored at −80°C. Cryosections were cut on a cryostat (Cryostar NX70, Thermo Scientific) and stored at −20°C. Eyes were sectioned at 20 µm thickness (anterior to dorsal plane), with sections maintained from approximately 200 µm nasal to approximately 200 µm temporal of the optic nerve head ($n = 3$ eyes each for NT/NT, OHT/OHT, NT/OHT, and OHT/NT). Optic nerves for cryosectioning were maintained as pairs attached at the optic chiasm, and sectioned at 20 µm to generate longitudinal nerve sections ($n = 4$ optic nerves each for NT/NT, OHT/OHT, NT/OHT, and OHT/NT). Brains were serial sectioned (coronal plane) at 50 µm from −4 mm caudal of cranial landmark Bregma, to −8 mm caudal of Bregma to capture the entire dLGN and SC ($n = 3$ brains each [6 independent hemispheres] for NT/NT, OHT/OHT, NT/OHT, and OHT/NT).

Immunofluorescence

The antibodies used for immunofluorescence labelling are detailed in Table. The same immunofluorescent labelling protocol was followed for cryosections and flat mount retina with exceptions noted where relevant. Tissue was isolated using a hydrophobic barrier pen (VWR), permeabilized in 0.5% Triton X-100 in 1× PBS for 1 hour, blocked in 5% bovine serum albumin in 1× PBS for 1 hour, and primary antibody applied overnight at 4°C (see Table). Tissue was then washed for 5 × 5 minutes in 1× PBS, secondary antibody applied (1:500 in 1× PBS) for 4 hours at room temperature, and washed for 5 × 5 minutes in 1× PBS. DAPI nuclear stain (500 µg/mL stock; used 1:500 in 1× PBS) was applied for 10 minutes, the tissue washed for 5 minutes in 1× PBS, dried, and mounted using Fluoromount-G and glass coverslips (Invitrogen, Carlsbad, CA). For cryosections, tissue was air dried for 15 minutes and rehydrated in 1× PBS for 15 minutes before following the protocol described above. For microglia analysis, retinas were co-labelled with RBPMS and IsoB4. RBPMS counts are presented in Tribble et al.[25] IsoB4 microglia data are presented in the current manuscript.

Assessment of Neurodegeneration after OHT

Eyes for flat mount retina preparations ($n = 6$ NT/NT eyes, 6 OHT/OHT eyes, 5 NT/OHT eyes, and 5 OHT/NT eyes) all at the 14-day time point were maintained in fixative as globes for 2 hours before the retina was dissected free at the optic nerve head, the vitreous removed, and the retina flat mounted ganglion cell layer up on a coated glass slide (Superfrost+, Thermo Fisher). Retinas were labelled with antibodies against RBPMS and IsoB4,

and counterstained with DAPI. Flat-mounted retinas were imaged on a Zeiss Axioskop 2 plus epifluorescence microscope (Carl Zeiss Meditech, Jena, Germany) for the quantification of RGC densities. Six images per retina (original magnification 40×, 0.25 µm/pixel) were taken equidistant to the optic nerve head (1000 µm eccentricity). Images were cropped to 150 × 150 µm and RBPMS+ cells were counted using the cell counter plugin for Fiji.[26] Cell counts were averaged across the six images, and expressed as a density per 0.01 mm^2 (comparison by one-way analysis of variance [ANOVA] with Tukey's honest significant difference [HSD]).

Microglia Imaging and Quantification

All microglia images were acquired on a Zeiss LSM800-Airy (20×, 319.45 × 319.45 µm, 0.312 µm/pixel, *z*-stack). Imaging parameters were kept constant to allow comparison of microglial volume. For flat-mounted retinas labelled with IsoB4, RBPMS, and DAPI, four images were taken at 1500 µm superior, nasal, inferior, and temporal to the optic nerve head. In longitudinal optic nerve sections, IsoB4 was imaged proximal to the eye and proximal to the chiasm. Images of IsoB4, Nissl, and DAPI-labelled brain sections were acquired at the midpoint of the SC and dLGN respectively. Microglia from retina and brain regions were reconstructed manually in Imaris (version 9.3.1, Bitplane, Zurich, Switzerland) using the Filaments tool with automatic volume filling and *z*-depth. Parameters were kept constant for a direct comparison of volumes. Microscopy, reconstructions, and image analysis were performed by independent researchers and final reconstructions curated by an independent researcher. In the retina, microglia were classified to either the nerve fiber layer/ganglion cell layer (NFL/GCL) or inner plexiform layer (IPL) based on *z*-depth, using the lower boundary of RBPMS nuclei as the limit of the ganglion cell layer. In the retina, approximately nine microglia per image were reconstructed in the NFL/GCL on average ($n = 137$ NT/NT, 185 NT/OHT, 197 OHT/NT, 222 OHT/OHT) and approximately seven microglia per image in the IPL on average ($n = 92$ NT/NT, 134 NT/OHT, 160 OHT/NT, 170 OHT/OHT). In the brain, approximately five (SC) and approximately six (dLGN) microglia were reconstructed per image on average (SC, $n = 103$ NT/NT, 114 NT/OHT, 115 OHT/NT, 121 OHT/OHT; dLGN, $n = 123$ NT/NT, 116 NT/OHT, 138 OHT/NT, 130 OHT/OHT). For individual microglia, the total number of branch points, total process length, total process volume, and field area (area enclosed by connected filament terminals) were calculated automatically and exported from Imaris. The total process volume was normalized to total process length to distinguish microglia with large but thin processes from those with short but thick processes. A Sholl analysis was performed with the soma center as the origin point and an intersection distance of 3 µm. The area under the Sholl curve (Sholl AUC) was calculated. The effect of experimental condition on microglia morphology were explored as an average across retina (mean of variable by retina; one-way ANOVA with Tukey's HSD) and as individuals where the higher level grouping (i.e., which retina each microglia originates from) was controlled, thus decreasing the error induced by intraclass correlation. For the latter, a linear mixed effects model approach was used (see Wilson et al.[27]). We resolved the issue of the nonindependence of samples by assuming different random intercepts for each retina and a fixed conditional effect by group (experimental condition) using the *lme4* package in R.[28] *P* values were obtained for regression coefficients using the *car* package.[29]

In the GCL, individual microglia were grouped by unsupervised hierarchical clustering (HC) to define populations of increasing reactivity. HC was performed using Morpheus (https://software.broadinstitute.org/morpheus) where every microglia from the GCL was classified based on the five morphologic measurements described above. For HC, microglia were clustered using Euclidean distance (linkage method = *average*). Cluster compositions by microglia condition were calculated. *k*-means clustering was performed in R (The R Foundation, Vienna, Austria) where *k* was set to 4 (the number of clusters determined by HC), to separate morphologically distinct microglia within condition groups. Like-for-like clusters were compared across the groups (each treated as an independent sample; one-way ANOVA with Tukey's HSD).

In longitudinal optic nerve sections ($n = 4$ optic nerves for NT/NT, OHT/OHT, NT/OHT, and OHT/NT) an area of $312(x) \times 624(y) \times 12.25(z)$ μm^3 was cropped (to avoid including the optic nerve sheath). The whole channel corresponding with IsoB4 was reconstructed as a volume using the Surfaces automatic volume analysis tool in Imaris. Image thresholding was kept constant. Because adjacent cells were sometimes considered as one object by the Surfaces algorithm, the number of microglia within the same area was counted manually using the Imaris Spots tool (analyzed by one-way ANOVA with Tukey's HSD).

Quantification of Infiltrating and Reactive Immune Cells

Microglia and monocyte density was calculated by counting all microglia and monocytes in the image volume, taking the average of the four regions imaged, and expressing as n/0.001 mm^3 (n = 6 NT/NT eyes, 6 OHT/OHT eyes, 5 NT/OHT eyes, 5 OHT/NT eyes; n = 3 brains [six independent hemispheres] for NT/NT, OHT/OHT, NT/OHT, and OHT/NT). Microglia in the retina were classified to the NFL/GCL or IPL as above. Monocytes were considered to be fully amoeboid (with no dendritic processes) only for the purpose of distinguishing microglia and monocytes. Counts were performed in three dimensions and as such no cells residing within the blood vessel structures were considered. We cannot preclude that the monocyte counts contain fully amoeboid microglia, nor that microglia counts contain microglia-like monocyte-derived macrophages, which could distort the true numbers of these cells. Microglia and monocyte soma center positions were recorded and related to RBPMS+ nuclei centers in the retina. For each microglia, nearest neighbor distances (NND) to the nearest microglia and neuron (RBPMS+ in the retina) were calculated in R using the *nndist* function in the spatstat package.[30] Monocyte NND was calculated in the same way. NNDs were compared across individual microglia (each treated as an independent sample; one-way ANOVA with Tukey's HSD) and using a linear mixed model accounting for group effects). Gliosis was determined by glutamine synthetase (GS) staining in the retina (cryosections; n = 3 eyes for NT/NT, NT/OHT, OHT/NT, and OHT/OHT). GS labelling was quantified by average pixel intensity and space filling assessed by fractal measurement (Fractal box count; Fiji, using boxes of size 2, 3, 4, 6, 8, 12, 16, 32, and 64).

Flow Cytometry Analysis of Microglia and Monocyte Populations

To assess the retinal microglia and monocytes numbers, at day 3 rats were euthanized as described elsewhere in this article (n = 7 NT/NT eyes, 8 OHT/OHT eyes), whole retinas dissected free from eyes cups under ice-cold HBSS, and dissociated in dispase in 1× HBSS (Corning Inc., Corning, NY) at 37°C and 350 RPM on an Eppendorf ThermoMixer C (Eppendorf, Hamburg, Germany). Cell were blocked with 1% bovine serum albumin in 1× HBSS for 1 hour and stained with antibodies against CD11b/c, CD45, and CD90.1. Cell numbers were assessed on a BD Influx equipped with 488, 561, 641 and 405 nm lasers. Gates were set based on FS versus SS and viability dye exclusion (LIVE/DEAD Aqua, Invitrogen). Microglia were identified as CD11b/c$^+$/CD45^{lo}/CD90.1$^-$ cells and monocytes identified as CD11b/c^{hi}/CD45^{hi}/CD90.1$^-$ cells (Table). Singlets were discriminated based on FS area versus pulse width. Cell samples were run for 600 seconds while mixing (accounting for approximately 25% of the total tissue homogenate) and data analyzed using FlowJo (FlowJo, LLC, Ashland, OR). Statistical analysis was performed using the Student t-test (unpaired, one-tailed following the Shapiro-Wilk test).

Cytokine Assay

A cytokine array analysis was performed to identify retinal or circulating factors that might influence immune activation in OHT and NT/OHT eyes. Rats were euthanized at day 14 and eyes enucleated (n = 4 eyes each for NT/NT, OHT/OHT, NT/OHT, and OHT/NT). Whole retina (without the optic nerve head) were dissected in HBSS and lysed in HBSS with protease inhibitors by ultrasonication (Vibra-Cell; Sonics & Materials, Newtown, CT). Samples were frozen at −80°C overnight, thawed, centrifuged, and protein quantification performed by Bradford assay. The array (Proteome profiler rat XL cytokine array kit; R&D Systems, Minneapolis, MN) was performed according to the manufacturer's instructions. We used 100 µg of protein for each sample and final membranes exposed to x-ray film for 2 seconds, 5 seconds, 10 seconds, 30 seconds, 1 minutes, 2 minutes, 5 minutes, 10 minutes, 20 minutes, and overnight (overexposure). The developed films were digitized and analyzed by densitometry after background subtraction (Fiji). Spots were analyzed in duplicate and normalized to the average of the three reference spot duplicates. The best exposure was determined by the strength of signal and lack of spot blurring. Statistical testing was performed in R, suing a multivariate ANOVA (Wilks' lambda) evaluating all cytokines as independent variables. This served as an initial screening tool identifying cytokines where variance was significantly altered across groups, which were then explored independently by ANOVA (with post hoc Tukey's HSD).

Statistical Analysis

All statistical analysis was performed in R. Data were tested for normality with a Shapiro Wilk test. Normally distributed data were analyzed by the Student t-test or ANOVA (with Tukey's HSD). Non-normally distributed data were transformed using

squared transforms; data that remained non-normally distributed were analyzed by a Kruskal-Wallis test followed Dunn's tests with Benjamini and Hochberg correction. Statistical tests are detailed at point of use. Unless otherwise stated, * = $P < 0.05$, ** = $P < 0.01$, *** $P < 0.001$, NS = nonsignificant ($P > 0.05$). For box plots, the center hinge represents the mean with upper and lower hinges representing the first and third quartiles; whiskers represent 1.5 times the interquartile range.

Results

Unilateral Glaucoma Does Not Cause Increased IOP or RGC Death in the Contralateral Eye

There was no significant difference between unilateral and bilateral NT eyes, or between unilateral and bilateral ocular hypertensive eyes (OHT) in terms of magnitude or duration of IOP increases (Figs. 1A, B). OHT resulted in significant loss of RGCs as identified by RBPMS labelling. The RGC density was decreased in both unilateral OHT/NT and bilateral OHT/OHT eyes compared with bilateral NT/NT and unilateral NT/OHT eyes, with no significant unilateral or bilateral effect in RGC death (Fig. 1C).

Retinal Microglia Demonstrate Increasingly Reactive Morphologies in Unilateral NT, Unilateral Ocular Hypertensive, and Bilateral Ocular Hypertensive Eyes

We performed volume reconstructions of individual microglia (n = 1297 microglia; Figs. 2 and 3) and assessed branching complexity, field area, and volume. Individual microglia were binned by their position within the retinal layers to either nerve fiber layer/ganglion cell layer (C) or IPL microglia. A comparison of morphology as a mean per retina demonstrated a significant decrease in branching density (Sholl AUC), the number of branches, total process length, and field area of microglia, with a significant increase in process volume in microglia from OHT eyes (OHT/NT or OHT/OHT) compared with NT eyes (NT/NT or NT/OHT), with no difference between NT unilateral or contralateral eyes (NT/NT vs NT/OHT) or OHT eyes (OHT/NT vs OHT/OHT; Supplementary Fig. S1). Individual mitochondrial morphology exhibited large variation within retinas across all conditions, indicating that multiple morphologic states existed within all experimental conditions and all retinas (Supplementary Fig. S1). A comparison of the morphology across experimental conditions (using a linear mixed model approach to account for intraclass correlation, where multiple microglia originate from the same sample) demonstrated a decrease in the branching density (Sholl AUC) from NT/NT for NT/OHT, OHT/NT, and OHT/NT and with increasing magnitude of the decrease through these groups (Fig. 2B). This pattern of decrease was also observed in the number of branches, total process length, and field area of microglia (Fig. 2B). The microglial volume was not significantly changed between NT/NT and NT/OHT eyes (Fig. 2B). When comparing OHT/NT and OHT/OHT, only the number of branch points and microglial volume were significantly different. These data quantitatively demonstrate morphologic changes consistent with increasing activation (retraction and increased volume)[31,32] occurring in microglia in OHT eyes. Microglia in NT eyes contralateral to OHT eyes demonstrate early reactive morphologies (retraction). These data support a population shift toward a more retracted morphology with increasing disease-related stress (microglia in NT/NT < NT/OHT < OHT/NT < OHT/OHT in morphology associated with activation).

In the IPL, the microglial morphology was not altered to the same degree as in the NFL/GCL (Fig. 3). Microglia from OHT eyes demonstrated significantly decreased Sholl AUC, number of branch points, total process length, and field area (Fig. 3B). The microglial volume was increased in OHT eyes compared with NT eyes (Fig. 3B). No significant difference in the Sholl AUC, number of branch points, total process length, field area, or volume were observed between the microglia from NT/NT and NT/OHT or between OHT/OHT and OHT/NT eyes (Fig. 3B). The microglia in the IPL also display activated morphologies in response to OHT, but do not show the same pattern in the magnitude of change with the same subtle population shift as in the NFL/GCL (OHT/OHT > OHT/NT > NT/OHT > NT/NT) (Fig. 3B).

To further examine this shift in the distribution of morphology by groups, we performed an HC of individual microglia in the NFL/GCL. Morphologic measures alone could group microglia by degree of activation (Fig. 4A). HC produced four clusters: cluster 1, a small cluster, n = 16, of NT/NT and NT/OHT microglia; cluster 2, n = 210, predominantly consisting of NT/NT and NT/OHT microglia reflecting microglia with resting morphology (63.5% and 51.4 % of total NT/NT and NT/OHT, respectively); cluster 3, n = 156, a mix of microglia from all four groups, representing morphologies related to early activation; and cluster 4, n = 359, predominantly OHT/NT and OHT/OHT microglia (67.5% and 85.6 % of total OHT/NT and

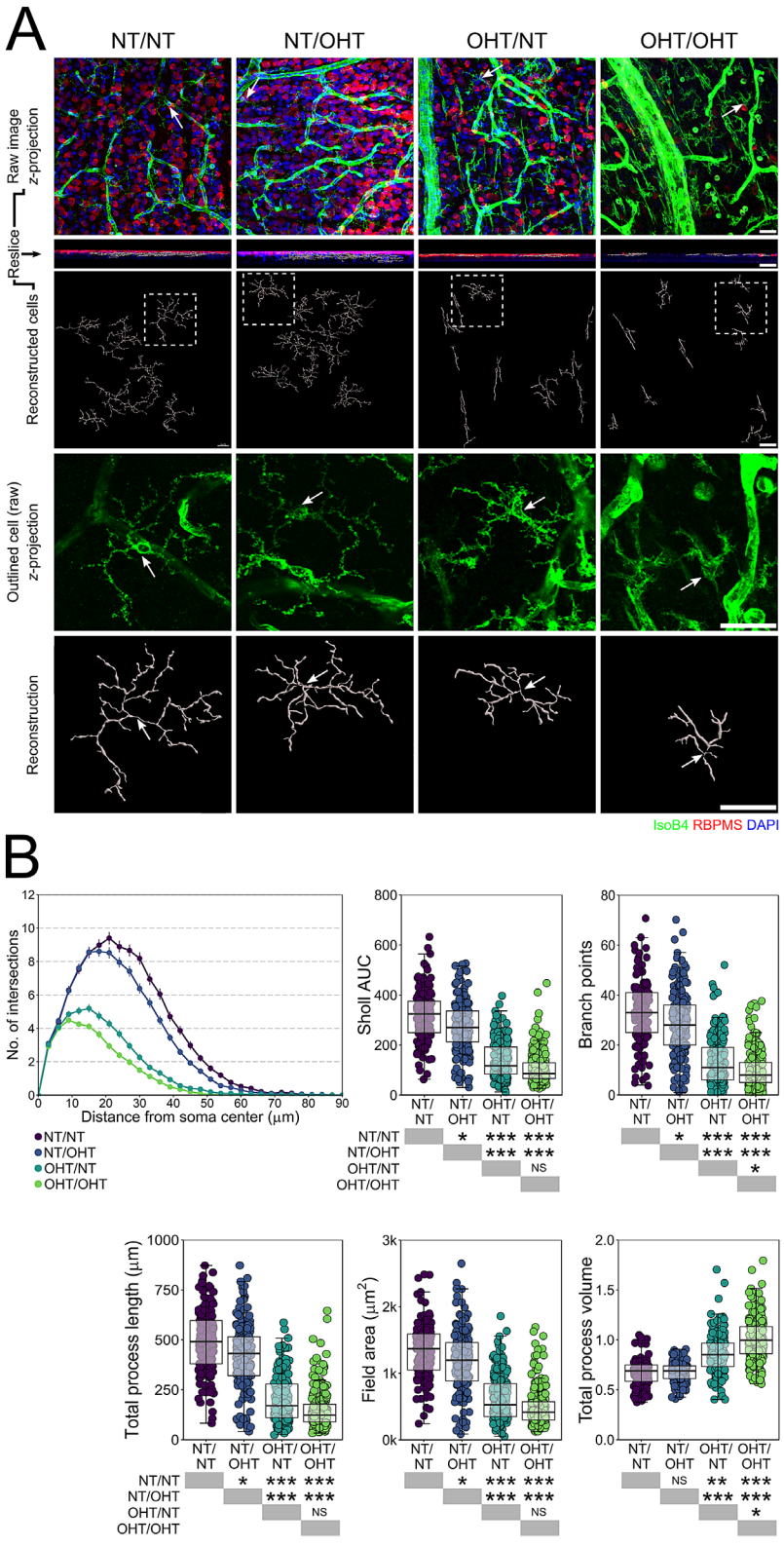

Figure 2. Direct or contralateral OHT results in increased microglia remodeling in the ganglion cell layer. (**A**) Morphologies of individual microglia from the NFL/GCL were assessed by high resolution confocal imaging and Imaris reconstructions (labels to left of image panel; $n = 137$ microglia in NT/NT, 185 in NT/OHT, 197 in OHT/NT, 222 in OHT/OHT, from $n = 5$ NT/NT eyes, 6 OHT/OHT eyes, 5 NT/OHT eyes, 5 OHT/NT eyes). (**B**) Multiple metrics of microglia morphology demonstrated significant changes in microglia between all groups suggesting progressive activation from NT/NT > NT/OHT > OHT/NT > OHT/OHT (retracted processes of increased volume). *White arrows* denote the microglia soma position; scale bars = 30 µm in A. $^*P < 0.05$, $^{**}P < 0.01$, $^{***}P < 0.001$. NS, not significant ($P > 0.05$).

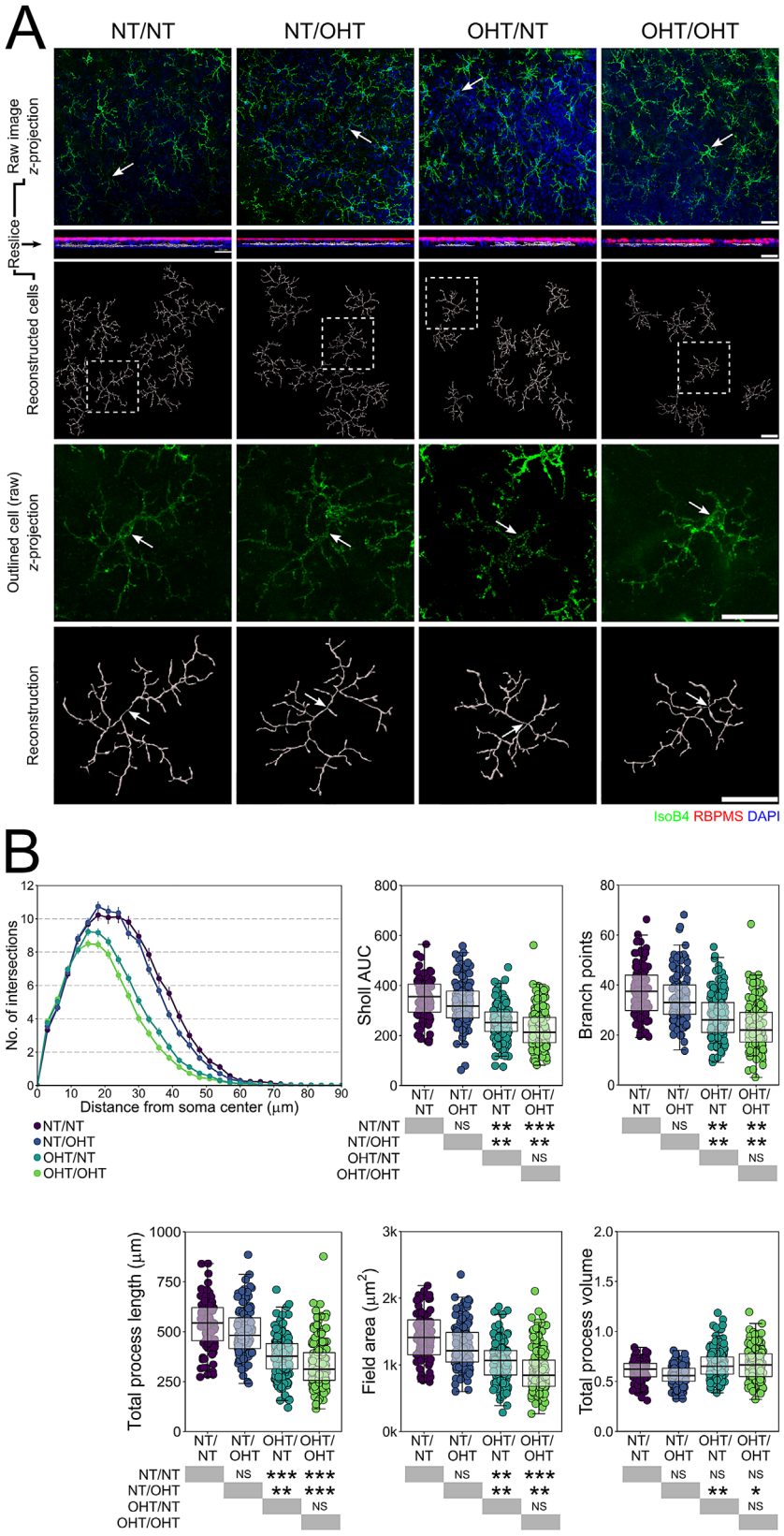

Figure 3. Direct, but not contralateral, OHT results in IPL microglia remodeling. (**A**) Morphologies of individual microglia from the IPL were assessed by high resolution confocal imaging and Imaris reconstructions (*labels to left of image panel; n* = 92 NT/NT, 134 NT/OHT, 160 OHT/NT, 170 OHT/OHT microglia). White arrows denote microglia soma position, scale bars = 30 µm in A, **P* < 0.05, ***P* < 0.01, ****P* < 0.001. NS, not significant (*P* > 0.05).

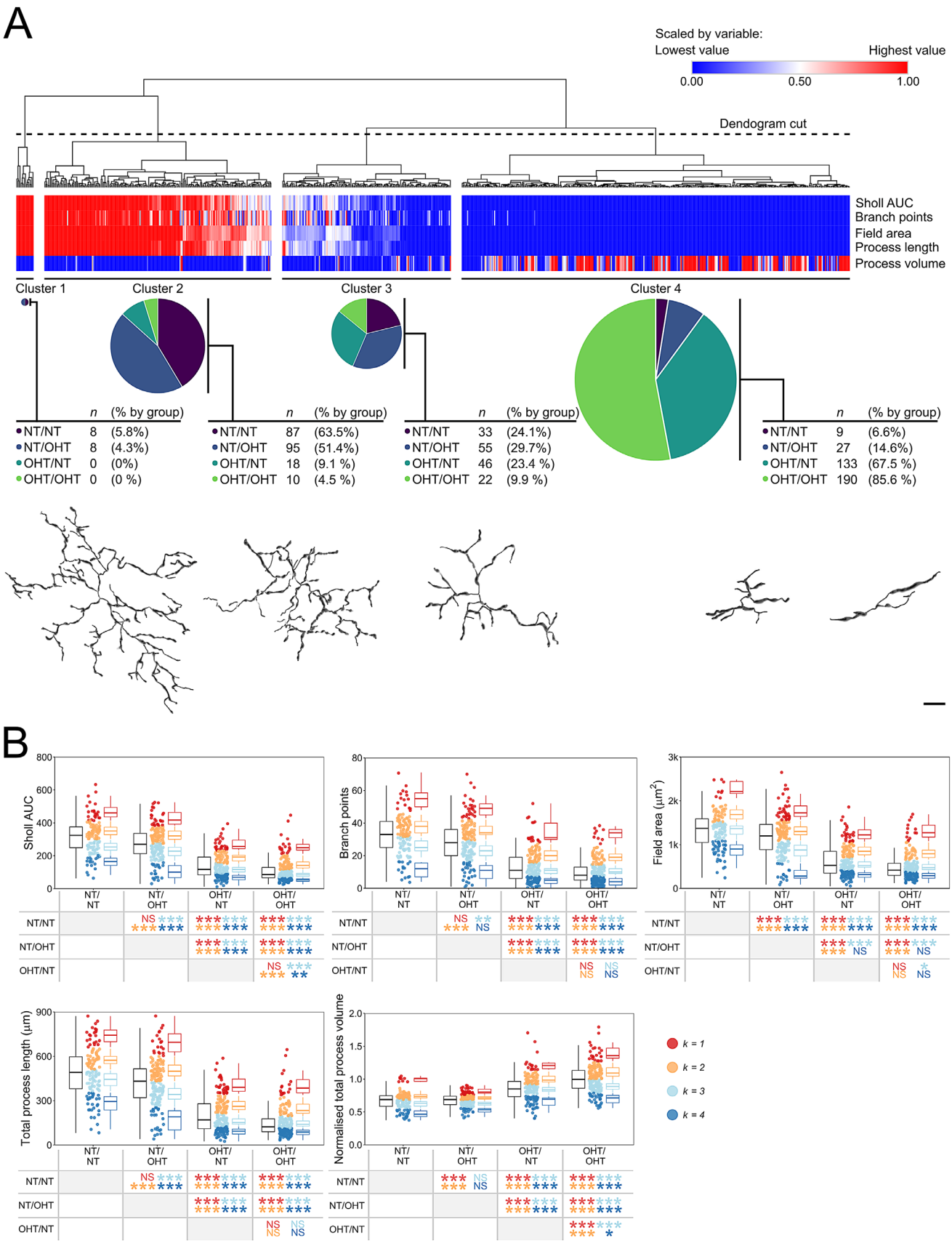

Figure 4. HC distinguishes activation state and disease groupings and identifies population shift in morphology in NFL/RGC layer microglia. (**A**) HC of NFL/GCL microglia metrics by Euclidean distance was used to cluster microglia morphologies, generating four independent clusters →

←
of microglia (clusters 1–4). The breakdown of each cluster is shown below the heatmap/dendrogram. Example cells belonging to each cluster, as shown below the cluster breakdown. Clusters represented groups of activation and demonstrates that microglial morphologic measurements can distinguish biologically meaningful groups of microglia independently of disease grouping. (**B**) HC clustering was used to inform a *k*-means clustering approach to stratify microglia within disease conditions to reflect the morphologic spectrum. Comparison of clusters demonstrated significant shifts in population toward a greater proportion of microglia whose morphologies are consistent with increased activation. Black boxplots to *left* represent all microglia per condition, colored boxplots to the *right* represent all microglia per cluster per condition and are colored individually (see legend). Scale bar = 10 µm. *$P < 0.05$, **$P < 0.01$, ***$P < 0.001$. NS, not significant ($P > 0.05$). Comparisons are colored to match the clusters.

OHT/OHT, respectively), representing retracted and condensed morphologies consistent with activation (Fig. 4A). The proportion of microglia from each of the conditions within each cluster suggested this shift in population. We next performed *k*-means clustering, informed by the HC, dividing each microglial population (by condition) in to four distinct clusters (because the unsupervised HC identified four morphologically distinct groups). The comparison across groups by cluster indicated that, globally, microglial shifted toward a distribution consistent with morphologies associated with greater activation, and fewer associated with resting states with a clear change between NT/NT and NT/OHT and between OHT/NT and OHT/OHT (Fig. 4B). Collectively, these data suggest that microglia exhibit varied morphologies within conditions, but that as a population they exhibit a graded shifted toward more retracted morphologies with increasing OHT (including from contralateral eyes).

Monocyte Infiltration Occurs Early after OHT

Increased numbers of microglia in the retina have been reported following OHT, as have mild increases in microglia number in NT eyes contralateral to OHT eyes. The microglia density was increased in the NFL/GCL in both OHT/NT and OHT/OHT eyes compared with NT/NT (Fig. 5A). There was no significantly detectable contralateral effect for either unilateral NT or OHT eyes in comparison with bilateral NT or OHT eyes (Fig. 5A). The microglia density in the IPL was less variable between groups, with only OHT/NT eyes showing a significant increase over other groups (Fig. 5A). A NND analysis revealed that the distance between the microglia in the NFL/GCL was smaller on average in OHT eyes than NT eyes, with no change in NT/OHT eyes compared with NT/NT eyes. The NND between NFL/GCL microglia was significantly shorter in OHT/OHT compared with ONT/NT eyes (Fig. 5B), indicating a trend between groups similar to that observed for microglial morphology. In the IPL, the NND between the microglia was not significantly altered (Fig. 5B), suggesting that the microglia here are largely distributed normally, as opposed to the pronounced changes in the NFL/GCL. Given that microglial density was substantially increased (a 2.8- to 3.5-fold increase), the NND was not increased to the same degree (a 1.6- to 2.4-fold increase), demonstrating that microglia remain well-distributed (i.e., avoid clumping/clustering). The NND between microglia and RGCs significantly increased in microglia from both the NFL/GCL and IPL under OHT in comparison with NT; there was no significant difference between NT or between OHT groups, indicating no contralateral effect influencing spatial microglial responses relative to RGCs (Fig. 5B). Because the increase in microglial density was concurrent with the decrease in RGC density, these data suggest that microglia are not clustering around surviving RGCs.

Extravasation and increased monocyte infiltration have been demonstrated as an early and persistent feature of glaucoma in animal models[33] and in post mortem human tissue,[2] and $CD45^{hi}$ monocytes are present in the retina in low numbers under normal physiologic conditions.[34,35] We observed IsoB4+ fully amoeboid cells (devoid of any dendritic processes) in the majority of retinas in all experimental groups, but demonstrate no significant change in the average monocyte density across experimental groups (Fig. 5C). We cannot preclude that the monocyte counts contain fully amoeboid microglia, which could distort the true numbers of these cells. A NND analysis demonstrated a significant decrease in distance between monocytes in OHT eyes compared with NT eyes (Fig. 5B). These data suggest a clumping of monocytes in OHT that may reflect recruitment rather than random transient migration into the retina (Fig. 5C). Monocyte infiltration has been shown to be an early event in glaucoma.[33] We counted retinal myeloid-derived cells by flow cytometry at an early time point (3 days after OHT induction, representing the peak IOP in the absence of RGC death in our experimental groups; Fig. 6). Monocytes, but not microglia, were significantly increased at this early time point in OHT compared with NT ($P < 0.01$; Fig. 6). This finding demonstrates early monocyte infiltra-

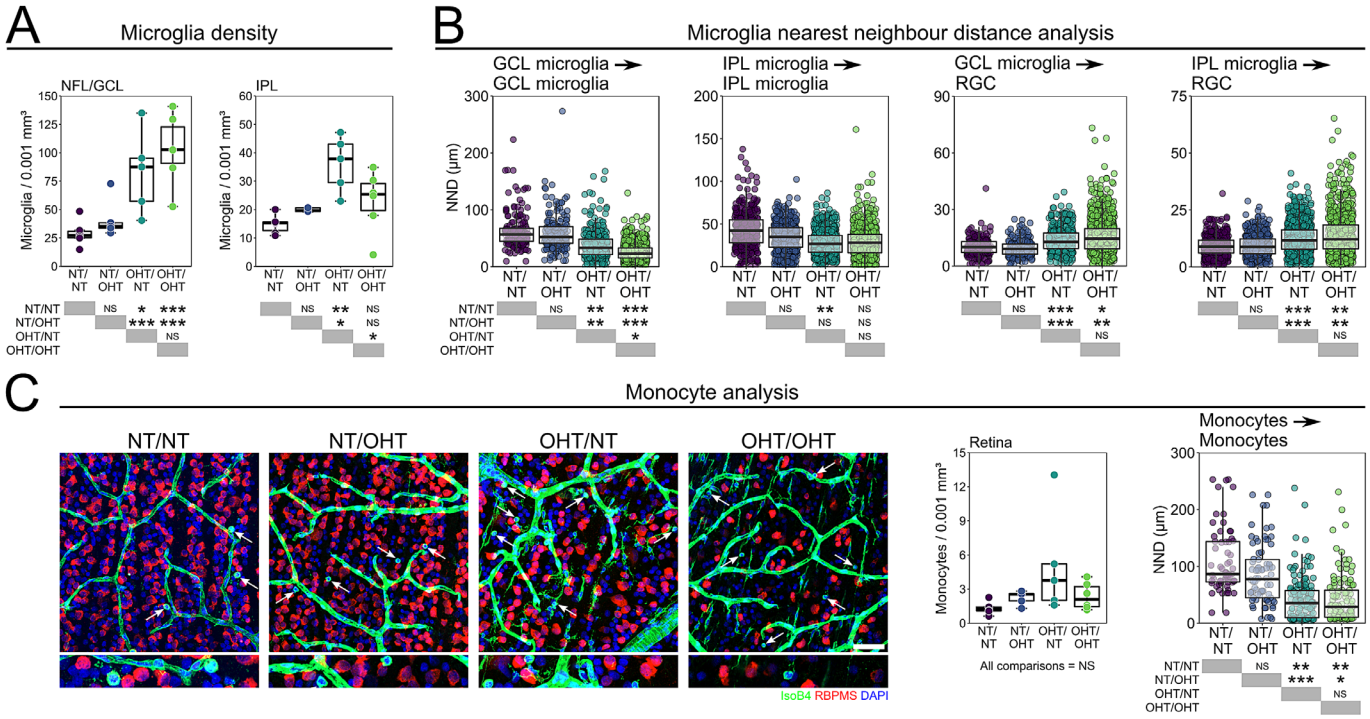

Figure 5. Microglia numbers increase in the retina following OHT. (**A**) After 14 days of OHT, microglia numbers were increased in both the NFL/GCL and IPL of the retina ($n = 6$ NT/NT eyes, 6 OHT/OHT eyes, 5 NT/OHT eyes, 5 OHT/NT eyes). (**B**) NND analysis demonstrates that microglia get closer to each other but are diffuse around RGCs suggesting that microglia do not cluster around surviving RGCs. (**C**) Ameboid monocytes were present in all conditions after 14 days of OHT (*white arrows*) with small NNDs suggestion monocyte clumping in local regions of damage. We cannot preclude that the monocyte counts contain fully amoeboid microglia, nor that microglia counts contain microglia-like monocyte derived macrophages which could distort the true numbers of these cells. Scale bars, 100 µm in C. *$P < 0.05$, **$P < 0.01$, ***$P < 0.001$, NS, not significant ($P > 0.05$).

tion in the absence of microglial proliferation. This early increase in monocytes and a late increase in microglia supports a hypothesis in which infiltrating monocytes become monocyte-derived microglia-like macrophages during glaucoma pathogenesis. Flow cytometry comparing NT/OHT and OHT/NT eyes may further explain the differences induced by contralateral injections, and will be an important future experiment.

No Detectable Müller Glia Activation after Ocular Hypertensive Glaucoma

Müller glia provide trophic and metabolic support to RGCs during times of stress, including glaucoma-related stresses.[36,37] Müller glia activation, identified by increased GS labelling, has been demonstrated in different animal models of glaucoma. To determine whether Müller glia activation was a component of glaucomatous neurodegeneration in this model, cryosections were labelled with antibodies targeting GS (Fig. 7A). An analysis of GS labelling in the NFL/GCL/IPL (representing the Müller glia association to RGC axon, soma, and dendrites) did not indicate significant Müller glial activation at this time point (Fig. 7B). Further analyses including greater number of samples and using other markers will be necessary to better understand contralateral responses in Müller glia.

Microglial Activation Extends into the Optic Nerve

Because RGC axonal loss with a concomitant loss of axon transport extended into the optic nerve in this model, we sought to determine whether this process was accompanied by microglial activation. Microglia were assessed in longitudinal optic nerve sections (Fig. 8A). Microglial counts demonstrated a significant increase in microglial density both proximal to the eye and proximal to the chiasm in OHT optic nerves compared with NT optic nerves (Fig. 8B). No contralateral change was observed in microglial density in optic nerves (Fig. 8B). Volume

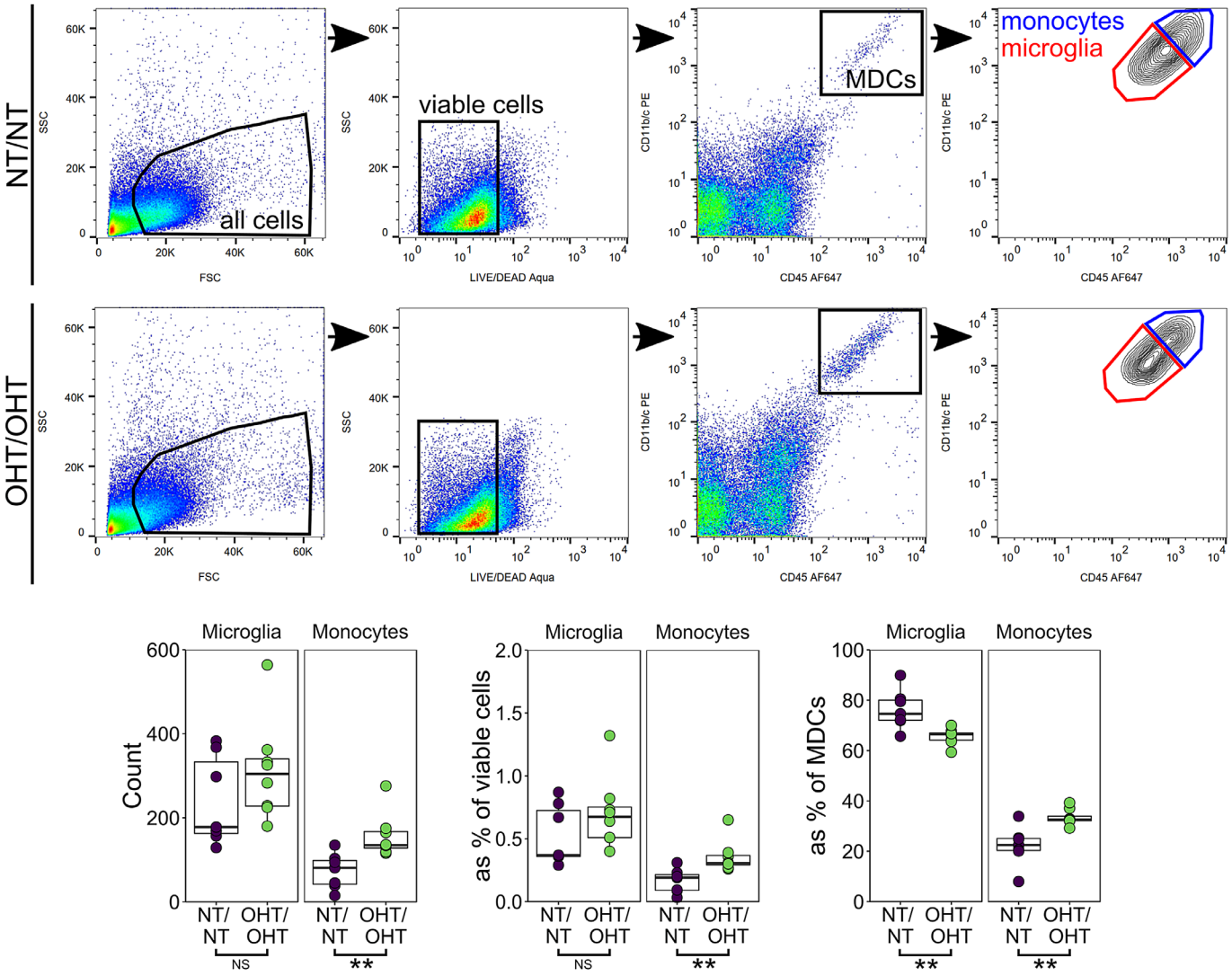

Figure 6. Monocytes enter the retina early after IOP elevation. To begin to assess whether this increase in microglia number was due to infiltrating monocytes entering the tissue and become microglia-like monocyte derived macrophages, whole retina homogenate was assessed by flow cytometry ($n = 7$ NT/NT eyes, 8 OHT/OHT eyes). Retinas were sampled at 3 days after injection (the point of peak IOP in this model). At this time point, the microglia numbers were not increased, although there was a significant increase in monocyte numbers (both by raw count and as a percentage of other cell types). MDCs, myeloid derived cells. For complete *n* please see Methods. $^{*}P < 0.05$, $^{**}P < 0.01$, $^{***}P < 0.001$. NS, not significant ($P > 0.05$).

reconstructions of whole IsoB4 content demonstrated the same trend, with significant increases in the OHT optic nerves compared with NT nerves, which was more pronounced proximal to the chiasm (Fig. 8B). A delineation of the individual microglia was not possible, and as such other microglial markers will be necessary to appreciate individual morphologic responses. Microglial activation was most evidently demonstrated at the chiasm where RGC axons from unilateral OHT eyes decussate, with the appearance of activated microglia following both optic tracts after the chiasm (Fig. 8C).

Microglia Are Activated in the dLGN and SC in Both Hemispheres, Irrespective of Unilateral or Bilateral OHT

Microglial activation in retinothalamic projections has been reported in animal models of glaucoma.[16,38] Brains were serial sectioned and microglia in central dLGN and SC were labelled (Figs. 9A–C). Microglial activation was evident in the dLGN across both hemispheres in all conditions compared with brains from NT/NT animals. Microglia demonstrated decreased branching complexity, number of branch

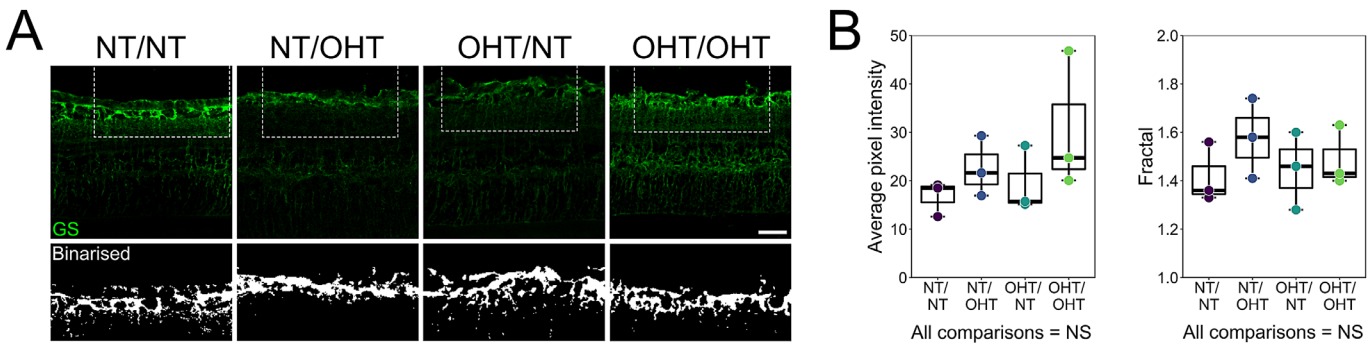

Figure 7. No activation of Müller glia identified by GS labelling. (**A**) Müller glia were labelled in cryosections by GS ($n = 3$ eyes for NT/NT, NT/OHT, OHT/NT, and OHT/OHT). GS content was assessed in the NFL/GCL/IPL by measuring average pixel intensity and by fractal analysis of binarized crops. (**B**) No significant difference in average pixel intensity or fractal was observed across groups, suggesting no gross Müller glia activation at this time point in this model. Scale bars = 50 µm in A. NS, not significant ($P > 0.05$).

points, total process length, and field area, and an increased volume (Fig. 9D). The dLGN contralateral to NT/OHT eyes (majority RGC input from NT eye) demonstrated significant changes in these measures compared with NT/NT dLGN (with the exception of volume), and no changes (with the exception of volume) when compared with microglia from fellow dLGN (contralateral to OHT/NT eyes; Fig. 9D), indicating that, largely, inflammation was not restricted, nor proportional, to the degree of RGC decussation. Microglia from OHT/OHT demonstrated significant changes from OHT/NT microglia in all metrics as well. Microglia counts demonstrated no significant increase in microglia density in the dLGN, suggesting activation in the absence of proliferation or infiltration (Fig. 9D). In the SC, the microglial morphology was also indicative of activation, with microglia demonstrating a significant decrease in branching complexity, number of branch points, total process length, and field area in both hemispheres from all conditions compared with NT/NT (Fig. 9E). In the SC, there was no significant difference in these measurements in microglia between hemispheres in unilateral animals, consistent with the findings in the dLGN (Fig. 9E). Microglia from OHT/OHT animals and both hemispheres of the unilateral animals were more similar in morphology than in the retina (Figs. 9D-E), suggesting that the degree of microglial activation in the SC is not contingent on the degree of dysfunctional and/or absent RGC input. Microglial density was increased in the SC in OHT/NT eyes, and highly variable in OHT/OHT eyes, suggesting proliferation or recruitment of the microglia in the SC (Fig. 9E). Because amoeboid monocytes were not observed in either the SC or dLGN, and that the SC and dLGN are not directly insulted by an elevated IOP, microglial proliferation is the most likely scenario. Both unilateral and bilateral OHT result in consistent microglial activation across both hemispheres of the visual thalami (i.e., neuroinflammatory signatures propagate even when only a small percentage of axons are damaged or dystrophic).

Upregulation of Cytokines in OHT and in Contralateral NT Eyes

Because NT/OHT eyes were free from detectable RGC dysfunction or neurodegeneration, but demonstrate substantial microglial inflammation in the corresponding optic nerve and in both terminal brain thalami, whole retinal lysate was probed for cytokine signals that could contribute to microglial activation (Fig. 10A). Of the 79 analytes assessed by cytokine array, 6 were identified as significantly altered across groups by multivariate ANOVA (Figs. 10B, C). These analytes were CNTF, fetuin A, FGF-1, galectin-3, ICAM-1 (CD54), and lipocalin-2. OHT eyes demonstrated a significant upregulation of CNTF compared with NT eyes. Fetuin-A and ICAM-1 were significantly increased in OHT/NT eyes compared with NT/NT eyes (Fig. 10C). Galectin-3 and lipocalin-2 were significantly increased in OHT/OHT eyes compared with NT/NT eyes (Fig. 10C). FGF-1 was significantly increased in NT/OHT eyes compared with NT/NT eyes (Fig. 10C). Determination of cytokine profiles at an earlier disease time point may reveal further changes between conditions and decrease the variance introduced by neurodegenerative processes. More time points will better delineate the temporal dynamics of inflammatory responses to OHT.

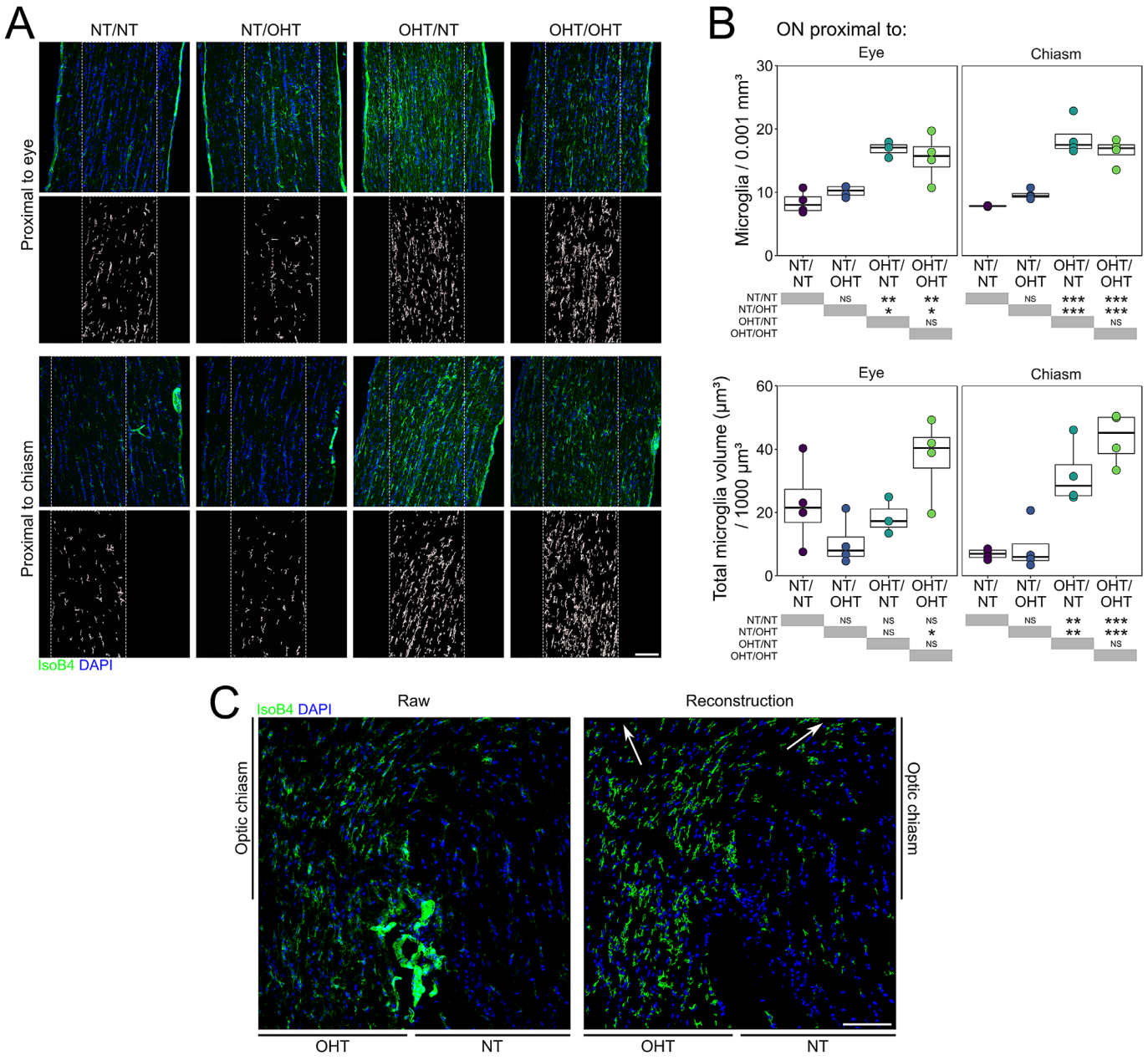

Figure 8. Microglia activation extends into the optic nerve and optic chiasm. (**A**) Optic nerves were transversally sectioned and overall microglial labelling was reconstructed (*insets*) and analyzed ($n = 4$ optic nerves for NT/NT, OHT/OHT, NT/OHT, and OHT/NT). (**B**) There exists significant microglia activation in the optic nerve proximal to the eye and proximal to the chiasm. (**C**) Microglial activation is most evidently demonstrated at the chiasm where the RGC axons from unilateral OHT animals decussate, with the appearance of activated microglia following both optic tracts post-chiasm (*white arrows* in reconstruction; *right*). Scale bars = 100 µm in A and C, $^{*}P < 0.05$, $^{**}P < 0.01$, $^{***}P < 0.001$. NS, not significant ($P > 0.05$).

Discussion

RGCs rely on supportive glia throughout their long projections to terminal visual thalami.[39] After periods of elevated IOP, these glia can become reactive, likely as an initial protective response that actually further compromises RGC survival.[3,40] Supporting this finding, complete ablation of microglia or monocytes only provides short-term neuroprotection in glaucoma.[33,41] In a recent study, almost complete depletion of resident microglia and infiltrating monocytes (using a PLX5622 and clodronate liposome combination treatment) failed to provide benefit in a more acute model (controlled optic nerve crush) and actually delayed axon regeneration after

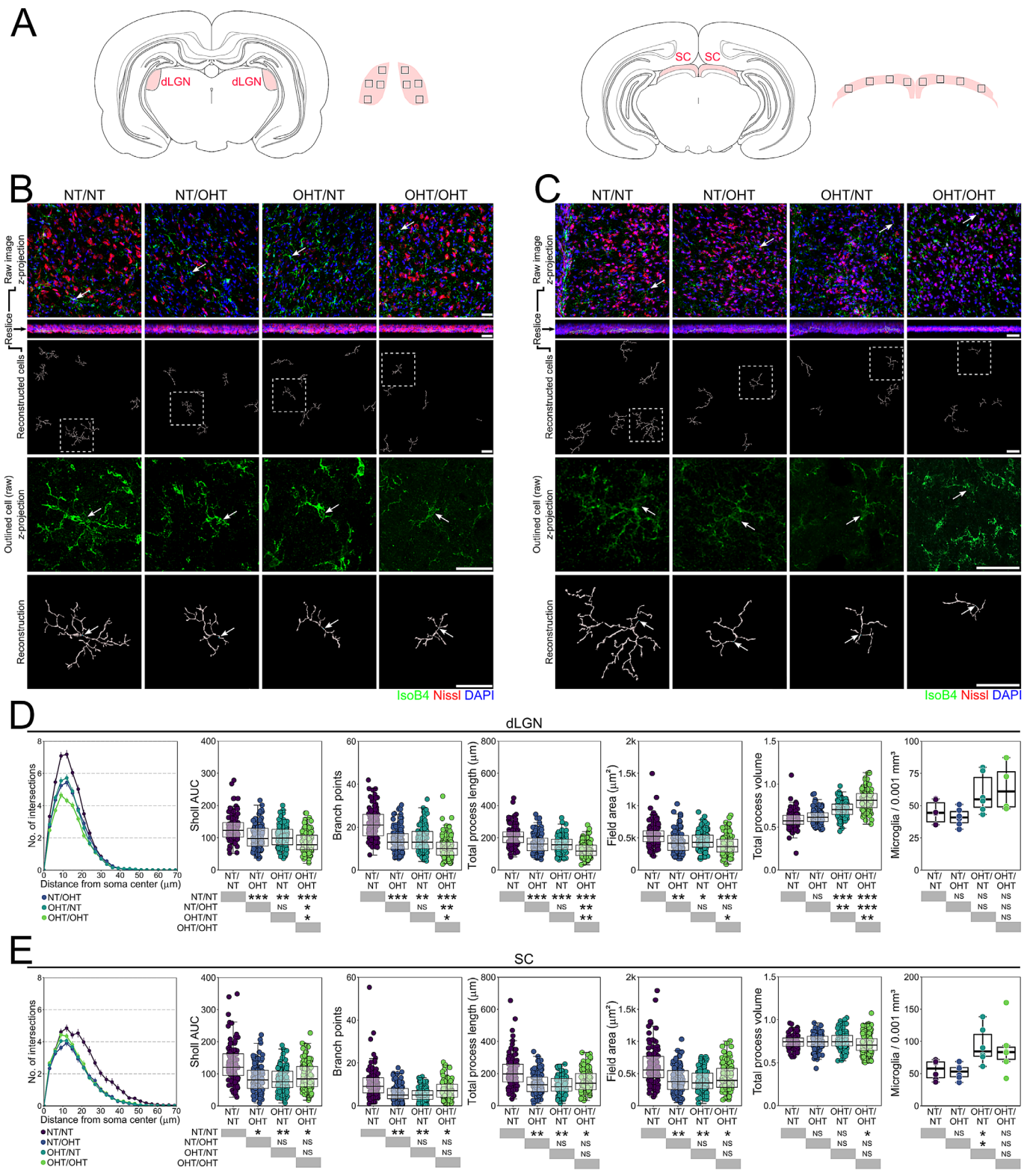

Figure 9. Microglia activation persists into terminal visual thalami following OHT. (**A**) Microglia were assessed from dLGN and SC sections (SC, $n = 103$ NT/NT, 114 NT/OHT, 115 OHT/NT, 121 OHT/OHT; dLGN, $n = 123$ NT/NT, 116 NT/OHT, 138 OHT/NT, 130 OHT/OHT; from $n = 3$ brains [6 independent hemispheres] for each condition). Regions of images are shown by *black inset boxes* in the schematics. Morphologies of individual microglia from the dLGN (**B**) and SC (**C**) were assessed by high-resolution confocal imaging and Imaris reconstructions (labels to left of image panel). (**D**, **E**) Multiple metrics of microglia morphology demonstrated significant changes in microglia morphology between NT/NT and all other groups (D shows dLGN, E shows SC). These results were more binary (i.e., damage to a single retina drives neuroinflammatory →

←

insults to both terminating hemispheres), suggesting that neuroinflammatory signatures propagate even when only a small percentage of axons are damaged or dystrophic. For complete *n* please see Methods. *White arrows* denote microglia soma position in B and C, scale bars = 30 µm in B and C, $*P < 0.05$, $**P < 0.01$, $***P < 0.001$. NS, not significant ($P > 0.05$).

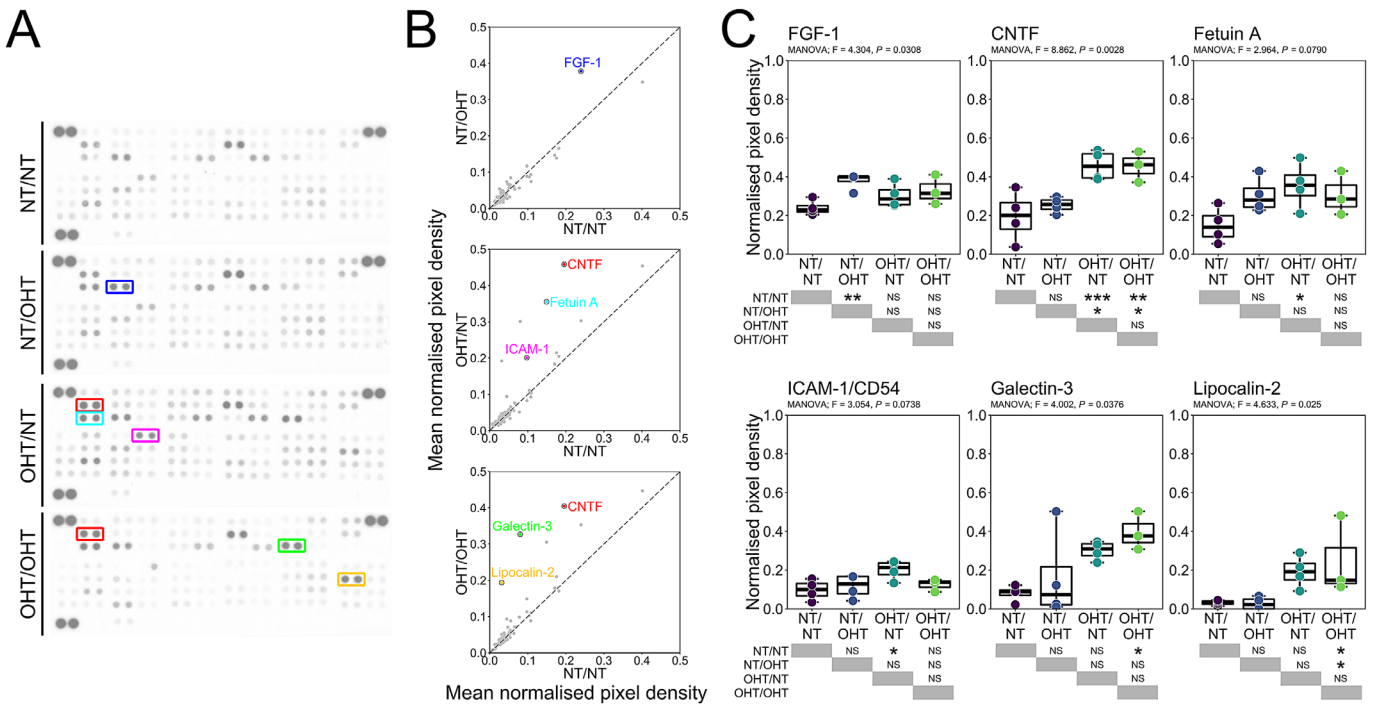

Figure 10. OHT drives neuroinflammatory cytokine expression in the retina. (**A**) To assess cytokine and chemokine expression in the retina after OHT, retinas were homogenized and assessed by protein array ($n = 4$ eyes for NT/NT, OHT/OHT, NT/OHT, and OHT/NT). (**B**, **C**) Densitometry analysis identified one changed cytokine (FGF-1) between NT/NT and NT/OHT groups, three changed cytokines (CNFT, fetuin A, ICAM-1) between NT/NT and OHT/NT groups, and three changed cytokines (CNTF, galectin-3, lipocalin-2) between NT/NT and OHT/OHT groups. All cytokines were increased compared with NT/NT groups and may represent ideal candidates for further experimentation or as biomarker candidates. $*P < 0.01$, $**P < 0.05$, $***P < 0.01$. NS, not significant ($P > 0.05$).

lens injury-induced RGC axon regeneration.[42] In the present study, quantification of the microglial morphology demonstrates retracted morphologies and an increased process volume, consistent with activation from a resting state.[31,32] Activated morphology persisted throughout the retina, optic nerve, and brain, mirroring RGC dysfunction that extended along the trajectory of the axon. Microglial morphology is highly variable in normal and diseased tissues, but as a population this shifts toward increasingly retracted and voluminous processes. This shift occurs as a gradient with increasing neurodegenerative and neuroinflammatory insult, where the effect in mild in NT eyes contralateral to the ocular hypertensive eye (no direct neurodegenerative insult) and greatest in bilateral OHT. Microglia in the GCL/NFL displayed this graded response (i.e., differences between unilateral and contralateral eyes), whereas those in the IPL did not, supporting a model of activation by the degree of direct insult in the retina.

Reciprocal signaling between the microglia and neurons plays an important role in defining microglia phenotypes.[43] The resting, nonactivated state, is in part controlled by CD200 and fractalkine (CX3CL1) signaling. CD200 is expressed by neurons and, through binding CD200R on microglia, maintains a resting state.[44,45] CX3CL1 is expressed in neurons and can be membrane bound and in a secreted form; it signals through its receptor on the microglia to maintain a resting state.[46,47] CD200 and CD200R expression changes early in glaucoma, whereas a loss of CX3CL1 signaling causes earlier axon transport dysfunction and in a DBA/2J mouse model of glaucoma.[48,49] Neurons also express markers of injury (e.g., surface expression of CCL21, which activates CXCR3 on microglia)[45,50,51] or of health (e.g., surface expression of CD47, the "do not eat me" signal).[52,53] Activated microglia exhibit increased expression of Toll-like receptors, complement receptor and components, and proinflammatory cytokines and chemokines. Microglia

and complement involvement in synapse elimination during the critical period and in neurodegenerative disease is well-established.[54–56] Complement components are upregulated in glaucoma in animal models and in human tissue, which play a critical involvement in synaptic pruning in glaucoma, and altered RGC survival through its manipulation.[57–64] This reciprocal relationship between microglial activation and neuronal dysfunction may underlie why microglial activation is so robust in the SC and dLGN, even in the absence of direct insult from OHT (e.g., direct IOP and vascular compromise).

We confirmed quantitatively the observation of activated microglia in NT eyes contralateral to OHT eyes. In these eyes, as in the brain, activation occurs in the absence of a direct OHT insult. The source of microglial insult is therefore either systemic or neuron derived. We observed no significant change in the IOP in NT/OHT eyes over NT/NT eyes. We also demonstrated no detectable RGC loss in the retina in NT/OHT eyes (and therefore did no additional assessment of other neurodegenerative parameters, e.g., axon counts, in these eyes). In the rat, decussation at the chiasm of approximately 90% of axons to the SC and dLGN contralateral to the eye of origin leaves approximately 10% of RGC axons projecting ipsilaterally. Significant microglial activation, therefore, persists along a substantial portion of these RGC axons and presents a proneuroinflammatory environment to otherwise healthy RGC terminals. It is possible that this interaction translates into activation at the somal end in the retina, although this remains to be validated experimentally. Supporting this notion, Sapienza et al.[16] demonstrated that both SC hemispheres in unilateral OHT demonstrated a significantly increased p-p38 pathway activation and oxidative stress characteristic of inflammation. Of note is the contralateral effect observed as the difference in activation between unilateral and bilateral OHT in the retina. This finding furthers the hypothesis that cumulative neuronal insult or systemic effects may drive activation to a greater degree in the retina. This same graded effect in the retina was not observed in the brain, where microglial activation was consistent across hemispheres, irrespective of whether the majority of input was from an OHT or NT eye in unilateral animals. However, there was evidence of greater activation in dLGN (but not SC) brain thalami receiving bilateral inputs from OHT eyes, as opposed to unilateral, suggesting cumulative effects. This difference between the dLGN and the SC may reflect the degree of input (20% compared with 80% of RGCs), suggesting an upper threshold of neuroinflammatory contralateral inputs before loss of a graded response. The degree of microglial activation, and its implications toward neuroglial signaling, neuroinflammatory environment, and RGC health, should caution against the use of the contralateral eye as a control in unilateral OHT animals and comparisons should not be made between the brain hemispheres.

Microglial proliferation and migration and monocyte infiltration have been reported in a number of glaucoma models and in human glaucoma.[2,12,33,41,49,65–67] We demonstrate that an early increase in monocytes, but not microglia, and a late increase in microglia, but not monocytes, occurs after sustained periods of OHT. The end-stage microglial counts were highly variable in retina and brain, demonstrating the need for a greater number of samples. Previous findings support an increase in microglia in the retina and the brain.[14,16] For the end-stage histology, where identification was based on IsoB4+ labeling and amoeboid morphology, we cannot preclude that the monocyte counts contain fully amoeboid microglia as well, which could distort the true number of infiltrating monocytes. These data suggest that monocytes infiltrate the retina and become microglia-like monocyte-derived macrophages, as has been reported in Alzheimer disease and other neurodegenerative diseases, as well as in retinal photoreceptor degeneration.[68–72] We have previously shown that vascular permeability is compromised in glaucoma, leading to increased extravasation of monocytes in addition to recruitment through vascular endothelial changes.[33,67] Definitively testing this hypothesis would require complex reporter alleles that are currently unavailable in the rat and, therefore, outside the scope of this study. Without these tools, it is not possible to identify microglia-like monocyte-derived macrophages that may have been included in the analysis of microglia morphology. We cannot preclude monocyte entry in to the optic nerve and brain thalami either; although we observed no obviously amoeboid cells, microglia-like monocyte-derived macrophages could be present in all tissues. Monocytes and other blood-derived immune cells have been noted in post mortem human glaucoma optic nerves.[2]

In our model, increased microglial activation and monocyte infiltration result in a significant proinflammatory environment. Cytokine and chemokine profiling in the retina identified a number of changes in OHT and in contralateral NT eyes. CNTF, fetuin A, FGF-1, galectin-3, ICAM-1 (CD54), and lipocalin-2 were all differentially elevated. CNTF, which can be released from microglia as a response to central nervous system injury, has demonstrated neurotrophic properties and increases RGC survival in glaucoma models.[73,74] CNTF also induces gliosis in Müller cells

and leads to the upregulation of proinflammatory cytokines and chemokines,[75–77] and as such its action is likely highly context dependent. Fetuin-A, a serum carrier protein, has been proposed as a biomarker of systemic inflammation, vascular disease, and neurodegenerative disease.[78–80] A decreased expression of fetuin-A correlates with the severity of cognitive impairment in Alzheimer's disease and fetuin-A–deficient mice demonstrate protection in experimental models of multiple sclerosis.[81,82] Galectin-3 mediates cell migration and adhesion, inflammatory cytokine release, and apoptosis and has been shown to activate microglia, astrocytes, monocytes, and other immune cells.[83] The plasma levels of galectin-3 correlate with Huntington's disease severity in patients and animals, and are associated with adverse outcomes in stroke and cerebral infarction.[84,85] The expression of galectin-3 was increased in Huntington's disease and genetic ablation of *Lgals3* is protective in animal models.[84] Microglial released galectin-3 can act as a ligand for Toll-like receptor 4, sustaining inflammatory responses.[86] Increased expression of galectin-3 has been detected in human glaucomatous donor tissue in the trabecular meshwork and optic nerve head in association with increased fibrosis.[87] *ICAM-1* is a glycoprotein that is expressed on leukocytes, macrophages and vascular endothelium. Its expression is upregulated in response to inflammatory stimuli (IL-1, tumor necrosis factor-α), where it functions as a ligand for integrins to facilitate endothelial binding and the transmigration of leukocytes.[88] *ICAM1* expression is increased in glaucoma patient leukocytes, but not blood plasma.[89,90] The upregulation of *ICAM1* is early and persistent in the optic nerve head and retina of DBA2/J mice, and is decreased by radiation, treatment which is highly protective for RGCs.[41] Lipocalin-2 is an antibacterial protein (acting through iron sequestration) that elicits proinflammatory responses and is implicated in a number of inflammatory and neurodegenerative diseases, including Stargardt disease and age-related macular degeneration in the retina.[91,92] *Lcn2* expression is also highly upregulated in DBA2/J glaucoma and in the rat hypertonic saline glaucoma model.[41,93] A recent Gene Expression Omnibus screen identified *LCN2* involvement in glaucoma pathogenesis.[94] Increased FGF-1 expression was identified in NT/OHT eyes. FGF-1 has demonstrated neuroprotective responses in neurodegenerative disease, but also activates astrocytes in the spinal cord, leading to proinflammatory responses.[95–98] Whether this response is neuroprotective or inflammatory and related to microglial activation warrants further exploration. Based on our findings, the earlier day 3 time point in which IOP peaks but neurodegeneration is not detected may offer an ideal time point to conduct additional cytokine profiling to support these findings at day 14, as well as additional microglia morphologic assessments to capture earlier responses. These proinflammatory events represent ideal candidates for further exploration using targeted knockouts, gene therapies, or antibody therapies in glaucoma.

Acknowledgments

The authors thank Monica Aronsson and Diana Rydholm for their assistance with animal husbandry and maintenance; St. Eriks Eye Hospital for financial support for research space, clinical histopathology, and animal facilities; the Knut and Alice Wallenberg Foundation and Karolinska Institutet for supporting the CLICK imaging facility; Annika van Vollenhoven at the Flow Cytometry Core Facility at the Karolinska Institutet Center for Molecular Medicine for flow cytometry; Charlotte Taul Brændstrup for assistance with Müller cell immunofluorescence; B. Paul Morgan for critical reading and editing of the article; and CITER (Cardiff Institute of Tissue Engineering & Repair) for supporting EK in the form of a research travel award.

Supported by Vetenskapsrådet 2018-02124 (PAW). Fight For Sight UK 512264 (JEM). Fight For Sight Denmark (MK). Pete Williams is supported by the Karolinska Institutet in the form of a Board of Research Faculty Funded Career Position and by St. Erik Eye Hospital philanthropic donations. Rupali Vohra is a part of the BRIDGE – Translational Excellence Programme at the Faculty of Health and Medical Sciences, University of Copenhagen (Novo Nordisk Foundation NNF18SA0034956).

JRT – designed and performed experiments, analyzed data, wrote the manuscript; EK – designed and performed experiments, analyzed data, wrote the manuscript; AO – performed experiments, analyzed data; FP – performed experiments, analyzed data; EL – performed experiments; RV – performed experiments; MK – provided resources, wrote the manuscript; HA – provided resources, designed experiments, wrote the manuscript; JEM – provided resources, designed experiments, wrote the manuscript; PAW – conceived, designed, performed experiments, analyzed data, wrote the manuscript. All authors read and approved the final article.

Disclosure: **J.R. Tribble,** None; **E. Kokkali,** None; **A. Otmani,** None; **F. Plastino,** None; **E. Lardner,** None;

R. Vohra, None; **M. Kolko,** None; **H. André,** None; **J.E. Morgan,** None; **P.A. Williams,** None

* JRT and EK contributed equally to this work.

References

1. Tham YC, Li X, Wong TY, Quigley HA, Aung T, Cheng CY. Global prevalence of glaucoma and projections of glaucoma burden through 2040: a systematic review and meta-analysis. *Ophthalmology*. 2014;121(11):2081–2090.
2. Margeta MA, Lad EM, Proia AD. CD163+ macrophages infiltrate axon bundles of postmortem optic nerves with glaucoma. *Graefes Arch Clin Exp Ophthalmol*. 2018;256(12):2449–2456.
3. Williams PA, Marsh-Armstrong N, Howell GR, Lasker/IRRF initiative on astrocytes and glaucomatous neurodegeneration participants . Neuroinflammation in glaucoma: a new opportunity. *Exp Eye Res*. 2017;157:20–27.
4. Cepurna WO, Kayton RJ, Johnson EC, Morrison JC. Age related optic nerve axonal loss in adult Brown Norway rats. *Exp Eye Res*. 2005;80(6):877–884.
5. Dräger UC, Olsen JF. Origins of crossed and uncrossed retinal projections in pigmented and albino mice. *J Comp Neurol*. 1980;191(3):383–412.
6. Jeffery G, Thompson ID. The effects of prenatal and neonatal monocular enucleation on visual topography in the uncrossed retinal pathway to the rat superior colliculus. *Exp Brain Res*. 1986;63(2):351–363.
7. Fukuda Y, Sawai H, Watanabe M, Wakakuwa K, Morigiwa K. Nasotemporal overlap of crossed and uncrossed retinal ganglion cell projections in the Japanese monkey (Macaca fuscata). *J Neurosci*. 1989;9(7):2353–2373.
8. Balkema GW, Pinto LH, Dräger UC, Vanable JW. Characterization of abnormalities in the visual system of the mutant mouse pearl. *J Neurosci*. 1981;1(11):1320–1329.
9. Ahmed AK, Guison NG, Yamadori T. A retrograde fluorescent-labeling study of direct relationship between the limbic (anterodorsal and anteroventral thalamic nuclei) and the visual system in the albino rat. *Brain Res*. 1996;729(1):119–123.
10. Dreher B, Sefton AJ, Ni SY, Nisbett G. The morphology, number, distribution and central projections of Class I retinal ganglion cells in albino and hooded rats. *Brain Behav Evol*. 1985;26(1):10–48.
11. Lund RD. Uncrossed visual pathways of hooded and albino rats. *Science*. 1965;149(3691):1506–1507.
12. Gallego BI, Salazar JJ, de Hoz R, et al. IOP induces upregulation of GFAP and MHC-II and microglia reactivity in mice retina contralateral to experimental glaucoma. *J Neuroinflammation*. 2012;9:92.
13. Kezic JM, Chrysostomou V, Trounce IA, McMenamin PG, Crowston JG. Effect of anterior chamber cannulation and acute IOP elevation on retinal macrophages in the adult mouse. *Invest Ophthalmol Vis Sci*. 2013;54(4):3028–3036.
14. Rojas B, Gallego BI, Ramirez AI, et al. Microglia in mouse retina contralateral to experimental glaucoma exhibit multiple signs of activation in all retinal layers. *J Neuroinflammation*. 2014;11:133.
15. Ebneter A, Casson RJ, Wood JP, Chidlow G. Microglial activation in the visual pathway in experimental glaucoma: spatiotemporal characterization and correlation with axonal injury. *Invest Ophthalmol Vis Sci*. 2010;51(12):6448–6460.
16. Sapienza A, Raveu AL, Reboussin E, et al. Bilateral neuroinflammatory processes in visual pathways induced by unilateral ocular hypertension in the rat. *J Neuroinflammation*. 2016;13:44.
17. Kongsui R, Beynon SB, Johnson SJ, Walker FR. Quantitative assessment of microglial morphology and density reveals remarkable consistency in the distribution and morphology of cells within the healthy prefrontal cortex of the rat. *J Neuroinflammation*. 2014;11:182.
18. Torres-Platas SG, Comeau S, Rachalski A, et al. Morphometric characterization of microglial phenotypes in human cerebral cortex. *J Neuroinflammation*. 2014;11:12.
19. Nimmerjahn A, Kirchhoff F, Helmchen F. Resting microglial cells are highly dynamic surveillants of brain parenchyma in vivo. *Science*. 2005;308(5726):1314–1318.
20. Wake H, Moorhouse AJ, Jinno S, Kohsaka S, Nabekura J. Resting microglia directly monitor the functional state of synapses in vivo and determine the fate of ischemic terminals. *J Neurosci*. 2009;29(13):3974–3980.
21. Li Y, Du XF, Liu CS, Wen ZL, Du JL. Reciprocal regulation between resting microglial dynamics and neuronal activity in vivo. *Dev Cell*. 2012;23(6):1189–1202.
22. Cserép C, Pósfai B, Lénárt N, et al. Microglia monitor and protect neuronal function through specialized somatic purinergic junctions. *Science*. 2020;367(6477):528–537.
23. Samsel PA, Kisiswa L, Erichsen JT, Cross SD, Morgan JE. A novel method for the

induction of experimental glaucoma using magnetic microspheres. *Invest Ophthalmol Vis Sci*. 2011;52(3):1671–1675.
24. Morgan JE, Tribble JR. Microbead models in glaucoma. *Exp Eye Res*. 2015;141:9–14.
25. Tribble JR, Otmani A, Kokkali E, Lardner E, Morgan JE, Williams PA. Retinal ganglion cell degeneration in a rat magnetic bead model of ocular hypertensive glaucoma. *Trans Vis Sci Tech.* 2021;10(1):21, https://doi.org/10.1167/tvst.10.1.21.
26. Schindelin J, Arganda-Carreras I, Frise E, et al. Fiji: an open-source platform for biological-image analysis. *Nat Methods*. 2012;9(7):676–682.
27. Wilson MD, Sethi S, Lein PJ, Keil KP. Valid statistical approaches for analyzing Sholl data: mixed effects versus simple linear models. *J Neurosci Methods*. 2017;279:33–43.
28. Bates, DM, Mächler M, Bolker B, Walker, S. Fitting linear mixed-effects models using lme4. *J Stat Softw*. 2015;67(1):48.
29. Fox, J, Weisberg, S. *An R Companion to Applied Regression*. Third edition ed. Thousand Oaks, CA: Sage; 2019.
30. Baddeley A, Rubak E, Turner R. Spatial Point Patterns: Methodology and Applications with R. 1st Edition. Boca Raton, FL: Chapman and Hall/CRC; 2015.
31. Stence N, Waite M, Dailey ME. Dynamics of microglial activation: a confocal time-lapse analysis in hippocampal slices. *Glia*. 2001;33(3):256–266.
32. Ransohoff RM, Perry VH. Microglial physiology: unique stimuli, specialized responses. *Annu Rev Immunol*. 2009;27:119–145.
33. Williams PA, Braine CE, Kizhatil K, et al. Inhibition of monocyte-like cell extravasation protects from neurodegeneration in DBA/2J glaucoma. *Mol Neurodegener*. 2019;14(1):6.
34. Paschalis EI, Lei F, Zhou C, et al. Permanent neuroglial remodeling of the retina following infiltration of CSF1R inhibition-resistant peripheral monocytes. *Proc Natl Acad Sci USA*. 2018;115(48):E11359–E11368.
35. Karlen SJ, Miller EB, Wang X, Levine ES, Zawadzki RJ, Burns ME. Monocyte infiltration rather than microglia proliferation dominates the early immune response to rapid photoreceptor degeneration. *J Neuroinflammation*. 2018;15(1):344.
36. Vohra R, Aldana BI, Skytt DM, et al. Essential roles of lactate in Müller cell survival and function. *Mol Neurobiol*. 2018;55(12):9108–9121.
37. Skytt DM, Toft-Kehler AK, Brændstrup CT, et al. Glia-neuron interactions in the retina can be studied in cocultures of Müller cells and retinal ganglion cells. *Biomed Res Int*. 2016;2016:1087647.
38. Wang X, Sam-Wah Tay S, Ng YK. Nitric oxide, microglial activities and neuronal cell death in the lateral geniculate nucleus of glaucomatous rats. *Brain Res*. 2000;878(1–2):136–147.
39. Vecino E, Rodriguez FD, Ruzafa N, Pereiro X, Sharma SC. Glia-neuron interactions in the mammalian retina. *Prog Retin Eye Res*. 2016;51:1–40.
40. Zeng HL, Shi JM. The role of microglia in the progression of glaucomatous neurodegeneration - a review. *Int J Ophthalmol*. 2018;11(1):143–149.
41. Howell GR, Soto I, Zhu X, et al. Radiation treatment inhibits monocyte entry into the optic nerve head and prevents neuronal damage in a mouse model of glaucoma. *J Clin Invest*. 2012;122(4):1246–1261.
42. Hilla AM, Diekmann H, Fischer D. Microglia are irrelevant for neuronal degeneration and axon regeneration after acute injury. *J Neurosci*. 2017;37(25):6113–6124.
43. Szepesi Z, Manouchehrian O, Bachiller S, Deierborg T. Bidirectional microglia-neuron communication in health and disease. *Front Cell Neurosci*. 2018;12:323.
44. Hoek RM, Ruuls SR, Murphy CA, et al. Down-regulation of the macrophage lineage through interaction with OX2 (CD200). *Science*. 2000;290(5497):1768–1771.
45. Biber K, Sauter A, Brouwer N, Copray SC, Boddeke HW. Ischemia-induced neuronal expression of the microglia attracting chemokine secondary lymphoid-tissue chemokine (SLC). *Glia*. 2001;34(2):121–133.
46. Nishiyori A, Minami M, Ohtani Y, et al. Localization of fractalkine and CX3CR1 mRNAs in rat brain: does fractalkine play a role in signaling from neuron to microglia? *FEBS Lett*. 1998;429(2):167–172.
47. Maciejewski-Lenoir D, Chen S, Feng L, Maki R, Bacon KB. Characterization of fractalkine in rat brain cells: migratory and activation signals for CX3CR-1-expressing microglia. *J Immunol*. 1999;163(3):1628–1635.
48. Taylor S, Calder CJ, Albon J, Erichsen JT, Boulton ME, Morgan JE. Involvement of the CD200 receptor complex in microglia activation in experimental glaucoma. *Exp Eye Res*. 2011;92(5):338–343.
49. Breen KT, Anderson SR, Steele MR, Calkins DJ, Bosco A, Vetter ML. Loss of fractalkine signaling exacerbates axon transport dysfunction in a chronic model of glaucoma. *Front Neurosci*. 2016;10:526.

50. Dijkstra IM, Hulshof S, van der Valk P, Boddeke HW, Biber K. Cutting edge: activity of human adult microglia in response to CC chemokine ligand 21. *J Immunol*. 2004;172(5):2744–2747.
51. van Weering HR, de Jong AP, de Haas AH, Biber KP, Boddeke HW. CCL21-induced calcium transients and proliferation in primary mouse astrocytes: CXCR3-dependent and independent responses. *Brain Behav Immun*. 2010;24(5):768–775.
52. Lehrman EK, Wilton DK, Litvina EY, et al. CD47 protects synapses from excess microglia-mediated pruning during development. *Neuron*. 2018;100(1):120–134.e6.
53. van Beek EM, Cochrane F, Barclay AN, van den Berg TK. Signal regulatory proteins in the immune system. *J Immunol*. 2005;175(12):7781–7787.
54. Stevens B, Allen NJ, Vazquez LE, et al. The classical complement cascade mediates CNS synapse elimination. *Cell*. 2007;131(6):1164–1178.
55. Schafer DP, Lehrman EK, Kautzman AG, et al. Microglia sculpt postnatal neural circuits in an activity and complement-dependent manner. *Neuron*. 2012;74(4):691–705.
56. Rajendran L, Paolicelli RC. Microglia-mediated synapse loss in Alzheimer's disease. *J Neurosci*. 2018;38(12):2911–2919.
57. Miyahara T, Kikuchi T, Akimoto M, Kurokawa T, Shibuki H, Yoshimura N. Gene microarray analysis of experimental glaucomatous retina from cynomologous monkey. *Invest Ophthalmol Vis Sci*. 2003;44(10):4347–4356.
58. Kuehn MH, Kim CY, Ostojic J, et al. Retinal synthesis and deposition of complement components induced by ocular hypertension. *Exp Eye Res*. 2006;83(3):620–628.
59. Tezel G, Yang X, Luo C, et al. Oxidative stress and the regulation of complement activation in human glaucoma. *Invest Ophthalmol Vis Sci*. 2010;51(10):5071–5082.
60. Howell GR, Macalinao DG, Sousa GL, et al. Molecular clustering identifies complement and endothelin induction as early events in a mouse model of glaucoma. *J Clin Invest*. 2011;121(4):1429–1444.
61. Williams PA, Tribble JR, Pepper KW, et al. Inhibition of the classical pathway of the complement cascade prevents early dendritic and synaptic degeneration in glaucoma. *Mol Neurodegener*. 2016;11:26.
62. Harder JM, Braine CE, Williams PA, et al. Early immune responses are independent of RGC dysfunction in glaucoma with complement component C3 being protective. *Proc Natl Acad Sci USA*. 2017;114(19):E3839–E3848.
63. Bosco A, Anderson SR, Breen KT, et al. Complement C3-targeted gene therapy restricts onset and progression of neurodegeneration in chronic mouse glaucoma. *Mol Ther*. 2018;26(10):2379–2396.
64. Howell GR, Soto I, Ryan M, Graham LC, Smith RS, John SWM. Deficiency of complement component 5 ameliorates glaucoma in DBA/2J mice. *J Neuroinflammation*. 2013;10:76.
65. Bosco A, Steele MR, Vetter ML. Early microglia activation in a mouse model of chronic glaucoma. *J Comp Neurol*. 2011;519(4):599–620.
66. Joachim SC, Gramlich OW, Laspas P, et al. Retinal ganglion cell loss is accompanied by antibody depositions and increased levels of microglia after immunization with retinal antigens. *PLoS One*. 2012;7(7):e40616.
67. Williams PA, Braine CE, Foxworth NE, Cochran KE, John SWM. GlyCAM1 negatively regulates monocyte entry into the optic nerve head and contributes to radiation-based protection in glaucoma. *J Neuroinflammation*. 2017;14(1):93.
68. Fani Maleki A, Rivest S. Innate immune cells: monocytes, monocyte-derived macrophages and microglia as therapeutic targets for Alzheimer's disease and multiple sclerosis. *Front Cell Neurosci*. 2019;13:355.
69. Thériault P, ElAli A, Rivest S. The dynamics of monocytes and microglia in Alzheimer's disease. *Alzheimers Res Ther*. 2015;7(1):41.
70. Lund H, Pieber M, Parsa R, et al. Competitive repopulation of an empty microglial niche yields functionally distinct subsets of microglia-like cells. *Nat Commun*. 2018;9(1):4845.
71. Ronning KE, Karlen SJ, Miller EB, Burns ME. Molecular profiling of resident and infiltrating mononuclear phagocytes during rapid adult retinal degeneration using single-cell RNA sequencing. *Sci Rep*. 2019;9(1):4858.
72. Ma W, Zhang Y, Gao C, Fariss RN, Tam J, Wong WT. Monocyte infiltration and proliferation reestablish myeloid cell homeostasis in the mouse retina following retinal pigment epithelial cell injury. *Sci Rep*. 2017;7(1):8433.
73. Ji JZ, Elyaman W, Yip HK, et al. CNTF promotes survival of retinal ganglion cells after induction of ocular hypertension in rats: the possible involvement of STAT3 pathway. *Eur J Neurosci*. 2004;19(2):265–272.
74. Pease ME, Zack DJ, Berlinicke C, et al. Effect of CNTF on retinal ganglion cell survival in experimental glaucoma. *Invest Ophthalmol Vis Sci*. 2009;50(5):2194–2200.
75. Xue W, Cojocaru RI, Dudley VJ, Brooks M, Swaroop A, Sarthy VP. Ciliary neurotrophic factor

induces genes associated with inflammation and gliosis in the retina: a gene profiling study of flow-sorted, Müller cells. *PLoS One*. 2011;6(5):e20326.
76. Lin HW, Jain MR, Li H, Levison SW. Ciliary neurotrophic factor (CNTF) plus soluble CNTF receptor alpha increases cyclooxygenase-2 expression, PGE2 release and interferon-gamma-induced CD40 in murine microglia. *J Neuroinflammation*. 2009;6:7.
77. Kahn MA, Ellison JA, Speight GJ, de Vellis J. CNTF regulation of astrogliosis and the activation of microglia in the developing rat central nervous system. *Brain Res*. 1995;685(1–2):55–67.
78. Guo VY, Cao B, Cai C, Cheng KK, Cheung BMY. Fetuin-A levels and risk of type 2 diabetes mellitus: a systematic review and meta-analysis. *Acta Diabetol*. 2018;55(1):87–98.
79. Naito C, Hashimoto M, Watanabe K, et al. Facilitatory effects of fetuin-A on atherosclerosis. *Atherosclerosis*. 2016;246:344–351.
80. Jirak P, Stechemesser L, Moré E, et al. Clinical implications of fetuin-A. *Adv Clin Chem*. 2019;89:79–130.
81. Smith ER, Nilforooshan R, Weaving G, Tabet N. Plasma fetuin-A is associated with the severity of cognitive impairment in mild-to-moderate Alzheimer's disease. *J Alzheimers Dis*. 2011;24(2):327–333.
82. Harris VK, Donelan N, Yan QJ, et al. Cerebrospinal fluid fetuin-A is a biomarker of active multiple sclerosis. *Mult Scler*. 2013;19(11):1462–1472.
83. Arikawa T, Simamura E, Shimada H, Nakamura T, Hatta T, Shoji H. Significance of sugar chain recognition by galectins and its involvement in disease-associated glycosylation. *Congenit Anom (Kyoto)*. 2014;54(2):77–81.
84. Siew JJ, Chen HM, Chen HY, et al. Galectin-3 is required for the microglia-mediated brain inflammation in a model of Huntington's disease. *Nat Commun*. 2019;10(1):3473.
85. Nishikawa H, Suzuki H. Possible role of inflammation and galectin-3 in brain injury after subarachnoid hemorrhage. *Brain Sci*. 2018;8(2):30.
86. Burguillos MA, Svensson M, Schulte T, et al. Microglia-secreted galectin-3 acts as a toll-like receptor 4 ligand and contributes to microglial activation. *Cell Rep*. 2015;10(9):1626–1638.
87. Belmares R, Raychaudhuri U, Maansson S, Clark AF. Histological investigation of human glaucomatous eyes: Extracellular fibrotic changes and galectin 3 expression in the trabecular meshwork and optic nerve head. *Clin Anat*. 2018;31(7):1031–1049.
88. Williams MR, Luscinskas FW. Leukocyte rolling and adhesion via ICAM-1 signals to endothelial permeability. Focus on "Leukocyte rolling and adhesion both contribute to regulation of microvascular permeability to albumin via ligation of ICAM-1". *Am J Physiol Cell Physiol*. 2011;301(4):C777–C779.
89. Yeghiazaryan K, Flammer J, Orgül S, Wunderlich K, Golubnitschaja O. Vasospastic individuals demonstrate significant similarity to glaucoma patients as revealed by gene expression profiling in circulating leukocytes. *Mol Vis*. 2009;15:2339–2348.
90. Kang JH, Wiggs JL, Pasquale LR. A nested case control study of plasma ICAM-1, E-selectin and TNF receptor 2 levels, and incident primary open-angle glaucoma. *Invest Ophthalmol Vis Sci*. 2013;54(3):1797–1804.
91. Jha MK, Lee S, Park DH, et al. Diverse functional roles of lipocalin-2 in the central nervous system. *Neurosci Biobehav Rev*. 2015;49:135–156.
92. Parmar T, Parmar VM, Perusek L, et al. Lipocalin 2 plays an important role in regulating inflammation in retinal degeneration. *J Immunol*. 2018;200(9):3128–3141.
93. Ahmed F, Brown KM, Stephan DA, Morrison JC, Johnson EC, Tomarev SI. Microarray analysis of changes in mRNA levels in the rat retina after experimental elevation of intraocular pressure. *Invest Ophthalmol Vis Sci*. 2004;45(4):1247–1258.
94. Feng J, Xu J. Identification of pathogenic genes and transcription factors in glaucoma. *Mol Med Rep*. 2019;20(1):216–224.
95. Wei X, He S, Wang Z, et al. Fibroblast growth factor 1attenuates 6-hydroxydopamine-induced neurotoxicity: an in vitro and in vivo investigation in experimental models of Parkinson's disease. *Am J Transl Res*. 2014;6(6):664–677.
96. Guo ZH, Mattson MP. Neurotrophic factors protect cortical synaptic terminals against amyloid and oxidative stress-induced impairment of glucose transport, glutamate transport and mitochondrial function. *Cereb Cortex*. 2000;10(1):50–57.
97. Thorns V, Masliah E. Evidence for neuroprotective effects of acidic fibroblast growth factor in Alzheimer disease. *J Neuropathol Exp Neurol*. 1999;58(3):296–306.
98. Garré JM, Yang G, Bukauskas FF, Bennett MV. FGF-1 triggers pannexin-1 Hemichannel opening in spinal astrocytes of rodents and promotes inflammatory responses in acute spinal cord slices. *J Neurosci*. 2016;36(17):4785–4801.